An integrated hybrid-chip-fibre platform for the generation of mid-infrared light

By

Sobia Rehman

A thesis submitted to Macquarie University
for the degree of Master of Research
Department of Physics and Astronomy
October 2018

Examiner's Copy

This thesis is a presentation of my original research work. Wherever contributions of others are involved, every effort is made to indicate this clearly, with due reference to the literature, and acknowledgement of collaborative research and discussions. The material presented in this thesis is, to the best of my knowledge, original and has not been submitted in whole or part for a degree in any university.

_____

Sobia Rehman

Acknowledgements

All praises and thanks to Allah Almighty, The source of all knowledge and wisdom endowed to mankind whose blessing and exaltation flourish my thoughts and bestowed me with a potential and ability to contribute my humble submission to the ocean of knowledge.

Finally, the thesis is all done! I have spent a significant time and hardship to produce this thesis. By no means could I have done this alone and I must now have got a chance to acknowledge a few names who have helped me to improve as a researcher.

First and foremost, I wish to thank my principal supervisor **Dr. Alex Fuerbach** who opened the door for me and gave me the opportunity to pursue research at Macquarie University. His patient guidance and expertise in this field of Laser and Photonics has led me throughout my studies, without which none of the work in this thesis would have been possible. In addition, my co-supervisor **Dr. Darren Hudson**, who was always available around the lab to provide all the technical and expert advises. Despite having little to no experience in the field ended, I am heartily obliged to my supervisors who assured me that I could do this and took me on board as their student.

Besides supervisors, I would like to acknowledge the valuable inputs from my colleague and friends **Thomas Gretzinger** and **Gayathri Bharatan**, who were always ready for fruitful discussions which helped me to shape my research work.

I would especially like to thank **Dr. Joanne Dawson**, the Master of Research coordinator, for the timely helps she had extended during this program.

Now to the amazing colleagues. Dr. Michael Withford, Dr. Stuart Jackson, Dr.Peter Dekker, Dr. Simon Gross, Dr. Alex Arriola, Dr. Benjamin Johnston, Dr. RobertWoodward, Dr. Matthew Collins, Dr. Martin Ams, Dr. Toney Fernandez, Alex Stokes, Anita Verinder, Glen Douglass, Andrew Ross-Adams, Blacke Entwisle, Michelle Witford. It was a great pleasure to work with you all.

Taking a few steps back now, I am thankful to my parents for always encouraging and supporting in life. There are many choices we have in life, but choosing who to be born under is not one of them. There is no other doubt that I am absolutely blessed with great parents, siblings and family. And finally, last but not the least, my strength, my husband and kids who were always praying and raising my spirits to complete this task with the best of my abilities.

This work is a complete mixture of the above people's knowledge and experience, all intertwined, giving result to this thesis, and my growth as a baby researcher.

I thank you all from the core of my heart.

Sobia

Abstract

The laser is, without doubt one of the most important, discoveries that have been made in the last century and within a few decades, visible and near-infrared (IR) laser light has found a vast number of important applications in industry and research. The discovery of low-loss optical fibres was another revolutionary step that underpinned the rise of the global telecommunication industry.

The mid-IR region of the electromagnetic spectrum spanning from about 2 – 20 µm, has recently been identified as a powerful tool for sensing and medical applications due to the strong and highly specific –interaction of light at these wavelengths with molecules. However, while lasers based on silica-fibres have proven to be the most versatile and efficient light sources in the visible and near-IR, those glasses become virtually opaque at mid-IR wavelengths and new solutions are required. In this work, mid-infrared fibre lasers that are based on fluoride-glass optical fibres and on femtosecond laser-inscribed chalcogenide glass integrated chips are investigated. In detail, this project is aimed at studying the feasibility of fabricating a wavelength-selective 3-D integrated coupler in Gallium Lanthanum Sulphide (GLS) glass. The demonstration of the first fibre pigtailed 4-port device in the mid-infrared is a prerequisite the future realisation of the first fully integrated mid- infrared ring laser. This, in turn, would further open the possibility to develop monolithic all-fibre mode-locked lasers that are based on non-linearly coupled waveguide arrays.

Contents

List of Figures

List of Tables

1

Introduction

Lasers are at the heart of research nowadays.

The invention of the lasers proved to be a game changer for many applications. This scientific breakthrough had an enormous impact in various different areas of daily life ranging from electronics, photonics, medical surgery, clinical dentistry, sensing and imaging, laser spectroscopy to optical communication to only name a few. It's almost impossible to list each and every application that is based on the availability of laser light. This amazing device is still capturing people's imagination.

1.1 Main Objective

The main goal of this project was to design, fabricate and characterise an optical coupler in GLS glass (a chalcogenide material), and to investigate the fiber-to-fiber coupling efficiency of this device in combination with active heavy metal flouride glass (ZBLAN) fibres as well as silica pump fibres. This proposed chip/fibre architecture is monolithic and potentially highly efficient due to the possibility to achieve low cavity losses. To accomplish this task, a novel four-port coupler design was proposed

and tested. This device was modelled on commercially available optical components for the visible and near-infrared regions of the spectrum. The mid-infrared spectral region, is of great interest for many areas in science and technology as virtually all molecules exhibit strong and highly distinct absorption features in this wavelength range [1], making mid-infrared spectroscopy a powerful tool to identify and quantify molecules in a particular environment. In addition, the symmetric and asymmetric O-H stretching vibrations of liquid water has strong absorption at wavelengths 2.662 µm and 2.734 µm [2] shaping its convenience for laser surgeries of tissues. Despite these obvious potentials, mid-IR laser applications are still scarce because of the non-existence of integrated optical components. A recent investigation into a suitable sample material has shown, that glass chips based on ZBLAN are not suitable because of their limited Numerical Aperture [3]. In contrast, GLS glass has emerged as a promising candidate. This project focused on the linear properties of this glass, and in future, more work will be carried out to also exploit its non-linear characteristics.

The objective of this project was thus to investigate the feasibility of using femtosecond laser direct inscription for the fabrication of fibre-pig-tailed directional couplers in GLS. Those couplers are intended to become the building blocks for fully integrated mid-IR guided wave ring laser cavities to realise light sources that are free from bulk optical components and that can therefore be used in real-world applications outside a laboratory environment. Looking further afield, these chips could eventually also become essential components of figure-of-eight laser cavities [4] that allow the generation of ultrafast laser pulses.

1.2 Layout of the thesis

This thesis has been divided into five chapters.

This first introductory chapter presents the rationale and the motivation of this work.

Chapter 2 summarises the relevant background information about laser and optical fibres, as well as, the basic principles of fibre lasers.

Chapter 3 presents the overview of the femtosecond laser direct-write technique and explains its crucial importance for this project. In addition, its utilisation in future steps of this work is discussed. Finally, the chalcogenide material, Gallium Lanthanum Sulphide (GLS) is introduced as a highly promising substrate material.

Chapter 4 contains all experimental results, i.e the data obtained from the characterisation of the fabricated directional couplers and discusses the main outcomes and conclusions from this work.

Finally, the thesis ends with concluding chapter 5 that also present an outlook towards future work.

2

Background theory of mid-infrared fibre lasers

This chapter discusses the necessary background theory and provides an introduction to the theory of lasers, fibre lasers, their geometries and suitable doping materials for emitting mid-IR light.

2.1 Lasers

The term 'LASER' is an acronym that stands for *Light Amplification by Stimulated Emission of Radiation*. For all lasers, the essential requirements are an energy (pump) source, a gain medium and an optical feedback element to make an efficient laser cavity. There are multiple possible implementations and a very basic one is shown in Fig 2.1. The pumping mechanism excites the electrons in the gain medium to a higher energy state and on their transition back to the ground state they emit light. This signal can further be amplified by the addition of optical feedback,

provided for example by mirrors, to create what should be called more precisely a laser oscillator [5].

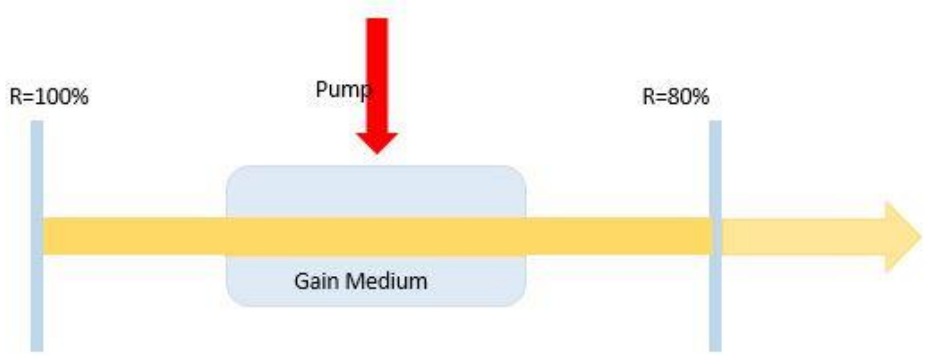

Figure 2.1: A basic laser system

Theoretically, stimulated emission was already predicted by Einstein in 1916 but the first experimental demonstration was only achieved in 1955 [6] at microwave wavelengths and hence the name “Maser” (Microwave Amplification by Stimulated Emission of Radiation) was coined. After the successful development of Masers, the same principle was transferred to the visible wavelength range (i.e visible light) and in 1960 the laser was born. After that, research into lasers flourished and still growing to date. Now a days a wide variety of lasers with different characteristic features exists and each laser has its unique applications. The first laser invented was a visible (red) laser in 1960 (ruby laser) and soon after infrared laser (near-IR Lasers like Nd:YAG but, also mid-IR lasers like CO_2) were successfully demonstrated. However, lasers operating in the important molecular finger print region around 3 - 10µm are still rare because only a few suitable gain materials exist and also due to the difficulty of finding suitable transparent materials in that wavelength range.

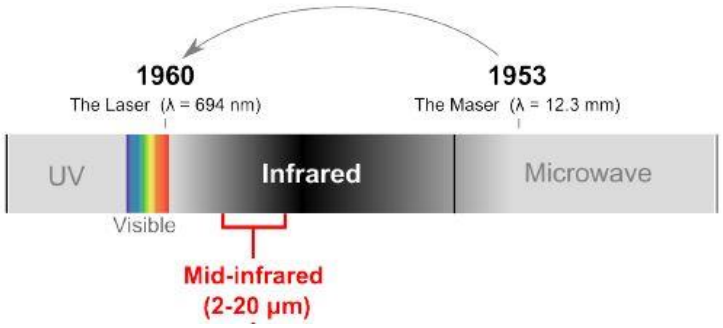

Figure 2.2: Electromagnetic spectrum showing the jump from Maser to Laser and the mid- infrared region in between [6]

However, as mentioned earlier in chapter 1, due to the importance of the mid-IR region of the electromagnetic spectrum, research into the development of light sources at this particular wavelength range is highly active.

2.2 Optical Fibres

The demand to create optical waveguides stemmed from the necessity to propagate light signals over large distances for communication and other purposes. An optical fibre is an elegant solution for this problem. An optical fibre is simply a long, tensile and translucent thread of glass or plastic with a thickness that is typically far less than the diameter of a human hair. It is constructed in such a way that the inner portion of the fibre which is known as its ***Core*** has a slightly higher refractive index than the surrounding material which is called the ***Cladding***. This allows a light signal to travel through the structure via ***Total Internal Reflection*** [7] as shown in the ray model of light below in Figure 2.3.

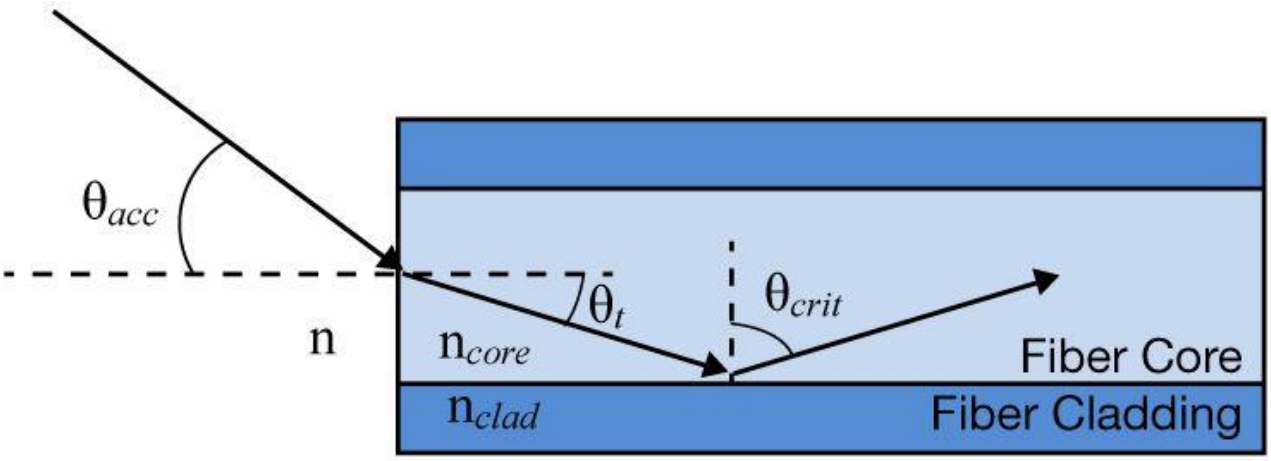

2.3: Principle of light propagation through an optical fibre [65]

Every transparent material combination is characterised by a specific value of the *critical angle* at which light rays that are passing from the optically denser to the less dense medium (i.e. from the medium with the higher refractive index to one with lower refractive index) refract at an angle of 90°. Beyond that point, at even larger angles of incident, no more refraction can occur and light rays are totally reflected back into the material, an effect that is known as a Total Internal Reflection (TIR). The conditions for total internal reflection therefore depend on the incident angle of light and on the critical angle of the two materials involved. In detail, these conditions are:

- The incident angle θ_t must be greater than the critical angle θ_{crit} ($90° - \theta_t > \theta_{crit}$)

and

- The refractive index of the core n_{core} must be greater than that of the cladding n_{clad} ($n_{core} > n_{clad}$).

For a step index fibre, the difference in refractive indices value defines an "acceptance cone" in which θ_{acc} is the angle of the acceptance cone. Only light rays entering at a set of angles smaller than θ_{acc} can only propagate through the core via total internal reflection while light rays outside the acceptance cone cannot be guided by the fibre as shown in Figure 2.3.

The sine of the half angle of this acceptance angle represents the Numerical Aperture (NA) which is a measure of *how much light can be collected by a fibre* and which solely depends on the values of refractive index of the core and the cladding and can be calculated by using the formula [8].

$$NA = \sqrt{{n_{core}}^2 - {n_{clad}}^2} \tag{2.1}$$

For a more accurate analysis of the light guiding process, the wave-nature of light has to be considered. Solving Maxwell's equations for a cylindrical geometry results in discrete solutions of light propagation within the fibre called 'Modes'. Another important property of an optical fibre is its 'V number' which is related to the number of modes that can be guided within the fibre. The lowest order mode which is called the *fundamental mode* that has a Gaussian-like intensity distribution is desired for most applications. The V number quantifies the number of modes that are supported by a particular fibre at a specific wavelength λ. It is calculated by using formula [8].

$$V = \frac{2\pi}{\lambda}\, a\, NA \tag{2.2}$$

where 'a' is the radius of the core of a fibre.

If V < 2.405, the fibre will support only one transverse mode (single-mode fibre), otherwise it is multi-mode. Thus, for a specific wavelength, the core radius and the numerical aperture are selected according to the mode requirement. A simple diagram that shows the transverse intensity distribution of different modes within a fibre is shown in Figure 2.4.

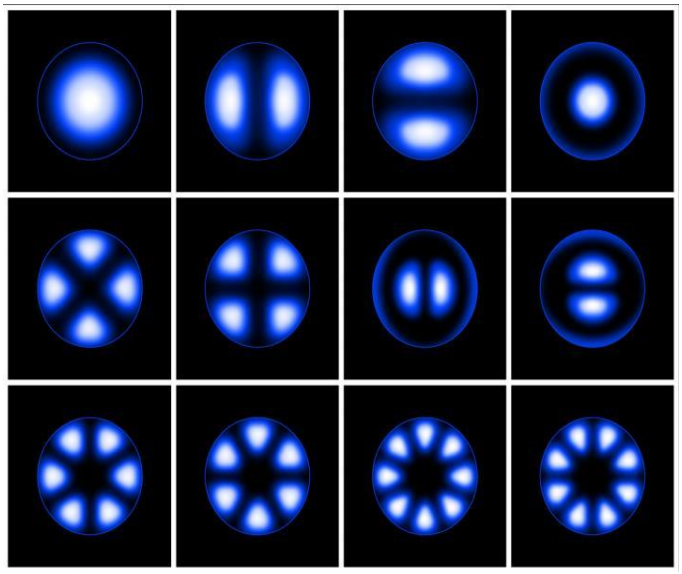

Figure 2.4: Different modes in fibres [66]

The most basic use of an optical fibre is to transmit light from one end to another and in fibre-optic communications, passive fibres are widely used to broadcast over long ranges as they can provide much larger bandwidths than electrical wires. Silica fibres are widely used in the telecommunication industry especially around the 1550 nm wavelength band. The selection of material for a fibre depends on the wavelength of light that is to be transmitted. One material can be ideal for a specific wavelengths, but the same material can be virtually opaque at other wavelengths. For instance, silica fibres are well suited for the visible and near IR region but above 2000 nm, the absorption losses increase rapidly and silica fibres become virtually opaque [9]. Thus, for wavelengths > 2000 nm, i.e. in the mid-infrared, different materials have to be used. In particular, fluoride and chalcogenide glasses are highly transparent in that region.

2.3 Fibre Lasers

Fibre lasers are excellent, powerful and unique waveguide resonant devices [10]. They work according to the same principles as discussed above and presented in Figure 2.1 and fibre-coupled laser diodes often act as the pump source. Further, active ions that are doped into the core of the fibre acts as the gain medium and optical feedback can be provided either by Fresnel Reflection off the perpendicularly cleaved flat ends of the fibre or by mirrors or Fibre Bragg Gratings (FBG's). Figure 2.5 below summarises these facts.

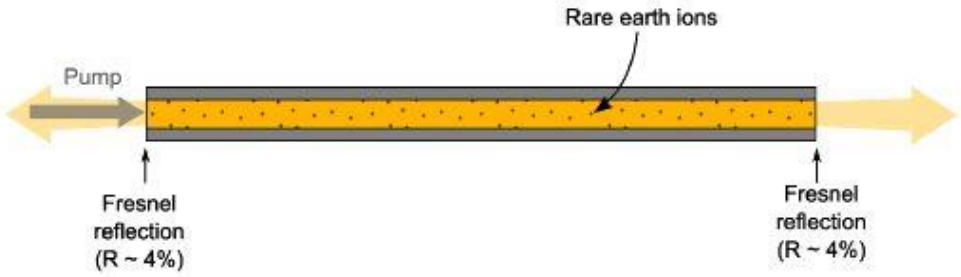

Figure 2.5: A Schematic diagram of a fibre laser[6]

The main advantages of fibre lasers are their compact size, their low weight and their monolithic design that makes them a particularly reliable source of laser light. Another advantage is that fibre lasers can produce very high power levels because of the large surface area of a fibre as compared to its volume, which provides a fibre laser system with self-cooling capabilities. In addition, fibre lasers are typically having the best beam quality among solid-state lasers [11].

In 1961, the first fibre laser was developed by E. Snitzer et al [12]. In this fibre, Nd-doped silicate glass was used as the active medium. Nowadays, the fabrication methods have been improved greatly such that fibres from ultralow-loss silicate and fluoride-based glasses can be manufactured that exhibit excellent qualities such as low background scattering, impurity deficiency and low material defects which give rise to enormous improvements in both quality and quantity of light that can be guided through the fibre. A very important invention in the area of active fibres was the double clad fibre. The reason for this innovation was that while a doped single-mode fibre is capable of generating a diffraction-limited output, this is only possible at relatively low power levels as the used pump sources are restricted to ones with diffraction-limited beam quality required to launch the pump light into the small core. In contrast, the use of multimode fibres (with a larger V-number and correspondingly higher number of propagating modes) results in a poor beam quality, yet the larger core relaxes the requirements for the pump diode. However, a high beam quality is required for most of the applications. This issue was solved by the invention of double-clad fibres in which the signal light travels in the doped core (typically single-mode) whereas the pump light propagates in a larger inner cladding that surrounds the core. The coupling of pump power is done by either directly injecting it into the inner cladding at the input end [13] or via side-pumping [14,15].

The pump light can be guided inside the inner cladding by surrounding it with an outer cladding (typically polymer) of an even lower refractive index. Part of the pump field then interacts with the core where it gets absorbed by the laser-active ions. The inner cladding usually has a very high numerical aperture to support a large number of propagation modes and hence enables efficient

coupling of pump light from multimode diodes. Figure 2.6 depicts light propagation inside a double clad fibre.

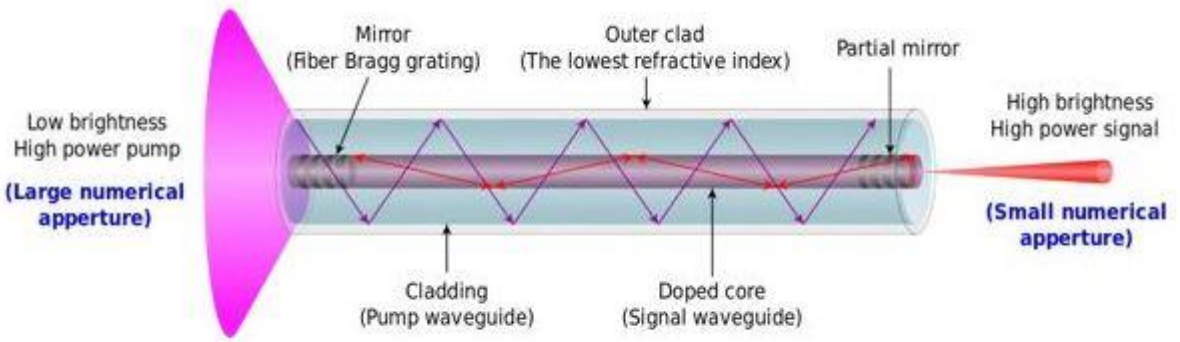

Figure 2.6: Propagation of light through a double cladding fibre [67]

By using multimode semiconductor diode lasers, high power optical excitation is feasible [16] and the brightness can be enhanced by many orders of magnitude [17]. Although doping the silicate glass with rare-earth cations adds Rayleigh scattering as compared to a passive fibre, this disadvantage can be neglected compared to the increase in gain.

2.4 Suitable dopant ions for the generation of mid-infrared light

An optical fibre that is capable of transmitting radiation in the infrared region of the electromagnetic spectrum is considered as an infrared optical fibre. IR optical fibres can broadly be divided into three categories:

- Glasses based on (i) Fluorides and (ii) Chalcogenides
- Crystalline materials like (i) Sapphire and (ii) Halides
- Hollow fibres having categories (i) Glass tube (ii) Hollow core photonic crystal fibres

All of these classes of fibres are important but the focus of this project lies on fluoride glass fibres (in particular ZBLAN) as they are highly transparent in the mid-IR region of the spectrum.

ZBLAN is a fluoride glass which can be used at longer wavelengths where Silica cannot be used any longer because of its intrinsic nature of absorption of signals above 2 µm as discussed above. This glass carries cations from heavy metals such as Zirconium. ZBLAN has a composition of ZrF_4-BaF_2-LaF_3-AlF_3-NaF and is considered as the most stable heavy metal glass and an excellent host for rare

earth ions. This glass is specifically used for its wide transparency window and low phonon energy (565 cm^{-1}) as compared to silica fibre (1100 cm^{-1}) [9]. The heavy ion constituents of ZBLAN lead to low phonon energy which further results in an increased infrared transmission of up to 4 µm as can be seen in Figure 2.7 which shows a comparison between the loss spectrum of silica and ZBLAN fibres. ZBLAN fibres can be doped with a variety of rare earth ions for applications in fibre lasers and amplifiers. Rare earth dopant ions in fluoride glasses strongly reduce the tendency for quenching processes caused by multi-phonon transitions which increases the lifetime of various metastable electronic levels, allowing the realisation of lasers based on various optical transitions. A comparison of fluoride fibres with other materials that are transparent in the mid-infrared region reveal their excellent properties such as low refractive index and low chromatic dispersion.

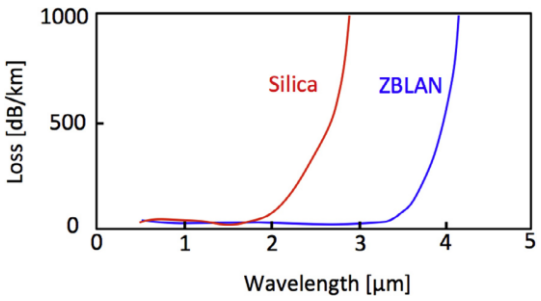

Figure 2.7: Comparison of propagation losses in silica and ZBLAN glass fibres [9].

Different research groups worked and are still working on fibre laser architectures for the generation of laser light in the mid-IR wavelength region. For example, it has been reported that a Thulium (Tm^{3+}) doped ZBLAN fibre laser can emit at 2.3 µm [18] and that an Erbium (Er^{3+}) doped ZBLAN fibre laser can emit at 2.7 µm and 3.5 µm [19,20]. Similarly, Holmium (Ho^{3+}) doped fibre lasers emitting at 2.9 µm, 3.2 µm, and 3.9 µm have been demonstrated in the past [19,20,23]. A very recent research paper has demonstrated emissions at 3.26 µm with Dysprosium (Dy^{3+}) doping [24]. An overview of the highest output power levels generated by fibre lasers at different wavelengths is presented in Figure 2.8.

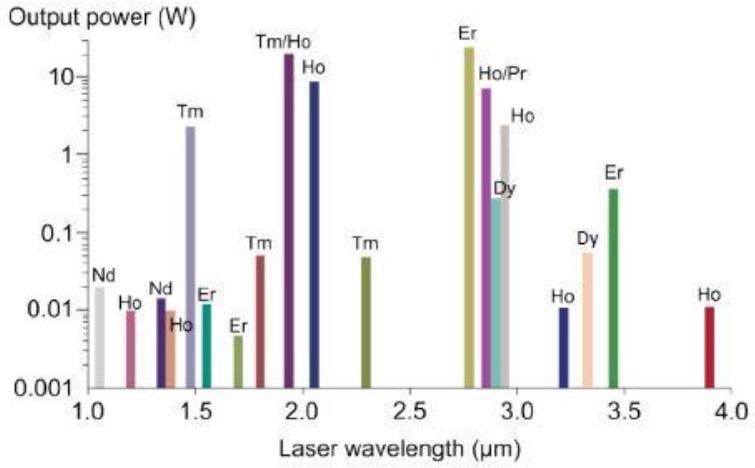

Figure 2.8: Successful dopants with ZBLAN glass to achieve lasing [3]

For the current project, a Ho^{3+} doped ZBLAN fibre was selected because while Er^{3+} doped fibres are capable of emitting at a wavelength of 2.8 µm, this wavelength overlaps with the high-absorption region of water vapour. On the contrary, Holmium (Ho^{3+}) fibre lasers overcome this issue by allowing the central emission wavelength to shift to 2.9 µm when pumped at a wavelength of 1.15 µm, thus avoiding water vapour absorption [25].

2.4.1 Holmium-doped ZBLAN Fibre Laser

Figure 2.9 shows the energy level diagram for Holmium-doped ZBLAN glass. When pumped at 1.15 µm, the transition from the $^5I_6$ level to the $^5I_7$ level resultsin the emission of light at a wavelength of about 2.9 µm which is of interest for this project. However, the longer lifetime of the lower laser level $^5I_7$ (12 ms) compared to the lifetime of the upper- laser level $^5I_6$ (3.5 ms) prevents population inversion and results in self-termination of this particular transition. This issue is resolved by adding another dopant ion i.e praseodymium (Pr), because this element has an energy level similar to the self-terminating level $^5I_7$ of Holmium. The Holmium ions can thus decay back to the ground state via multiphonon decay through a resonant energy process due to the praseodymium ions as represented in Figure 2.9 (b). This system efficiently emits light up to 3 µm with output power levels of multiple Watts [26,27].

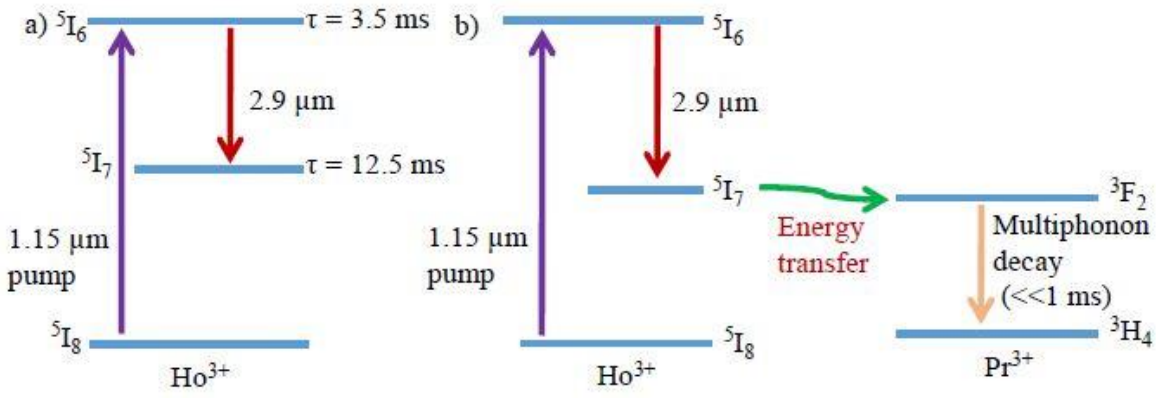

Figure 2.9: (a) Energy level diagram of Holmium ions

(b) Energy level diagram of Holmium ions after adding Praseodymium ion for quick decay via multiphonon scattering [3]

3

Ultrafast laser direct inscription technique

Soon after the advent of lasers, the field of ultrafast optics was generated by the demonstration of lasers with femtosecond pulse duration. Waveguide writing is one of the many important application of ultrashort-pulsed lasers. This chapter starts by discussing, the physical mechanisms of laser-matter interaction and the refractive index modifications that can be induced in transparent dielectric materials as a result. Furthermore, the exposure conditions required for producing observable variations in the properties of fabricated waveguides are discussed. Gallium Lanthanum Sulphide (GLS) is then introduced as a sample material for the fabrication of waveguides and couplers for the mid-IR and the design of a wavelength-selective evanescent coupler is introduced.

3.1 Femtosecond laser direct inscription

This very unique technique of fabricating optical and photonic structure was first discovered by Davis et al in 1966 [28] and has since then opened up a wide range of possible application. Using this writing method it is not only possible to inscribe optical waveguides but also micro-optics [29], micro-fluidics [30], micro-mechanics [31] circuitry all into all into a single substrate. The technique uses a femtosecond laser beam which is tightly focused inside a transparent sample that is placed on a computer-controlled motion translation stage to directly inscribe the above mentioned micro-structures. The sample material and the laser wavelength have to be selected in such a way that the photon energy of the laser light ($E_p = h\upsilon$, where 'h' is Plank's constant and 'υ' is the oscillation frequency of the light) is too low to directly excite an electron across the material band-gap or in other words the materials must not absorb the wavelength of femtosecond laser in a linear fashion. While there are also other photonic-device fabrication techniques available, the following advantages of the femtosecond laser direct-inscription technique made it the method of choice for our work. Firstly, the induced changes remain confined to the focal volume of the inscription beam and this confinement along with the 3-D translation of the substrate stage enables the design of complex structures in three dimensions. Secondly, due to the non-linear absorption that underpins this method, a wide variety of different material can be processed. Finally, this technique can be used to fabricate several different photonic devices into a single transparent substrate.

3.2 Laser-matter interaction

The interaction of laser light with a bulk material can result in different effects depending on factors like laser intensity, pulse duration, wavelength and frequency of light but also on material properties such as the type of the material (dielectric or polymer) and its absorption properties.

In transparent materials like glasses (chalcogenide glass GLS for the current project), electrons reside in the valence band and the conduction band is usually empty. These two bands are separated by a band gap energy E_g which is larger than the energy of a single photon of light and thus nonlinear absorption is required to promote electrons to the conduction band. There are two types of nonlinear absorption processes: ***photoionization*** and ***avalanche*** ionization.

3.2.1 Nonlinear photoionization

Photoionization is the direct excitation of an electron from the valence band to the conduction band by the laser field. Two mechanisms are possible depending on the frequency and intensity of the laser light; ***tunnelling ionization*** and ***multiphoton ionization***.

In ***tunnelling ionisation***, the coulomb potential that binds an electron to its nucleus is distorted by the electric field of the laser. Hence, the electron can tunnel through the resulting barrier to the conduction band as shown in Fig 3.1(b). This type of ionization is dominant when the laser field is strong and its frequency is low.

In contrast, in ***multi-photon ionisation***, 'n' number of photons interact with an electron at the same time to promote it to the conduction band as represented by Fig 3.1(a). For this process it is necessary that all the photons must interact with the electron simultaneously, therefore the likeliness of this process to occur strongly depends on the electric field strength. At high laser frequencies, multi-photon ionization is dominant.

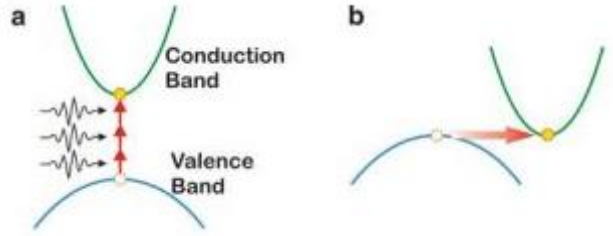

Figure 3.1: (**a**) Multiphoton Ionization (**b**) Tunnelling Ionization [32]

A parameter known as the Keldysh parameter (γ) can be used to quantitatively describe which type of ionisation is dominant [33]. It is defined as

$$\gamma = \frac{\omega}{e}\sqrt{\frac{m_e c n \epsilon_o E_g}{I}}$$

Where ω is the laser frequency

e is the charge of an electron

m_e is the mass of electron

c is the speed of light

ϵ_o is the vacuum permitivity

E_g is the band gap energy of the material

and I is the laser intensity at focus

If γ >> 1.5, the dominant process is Multiphoton Ionization and for γ << 1.5,Tunnelling Ionization is dominant. For γ ≈ 1.5, both processes provide a substantial contribution.

3.2.2 Nonlinear avalanche ionization

Avalanche Ionization depends on the presence of electrons in the conduction band. These (quasi-free) electrons can absorb multiple laser photons and thus continue to move to higher energy states,as shown on the left hand side of the Figure 3.2, until they gain sufficient energy to ionize other electrons from the valence to the conduction band.

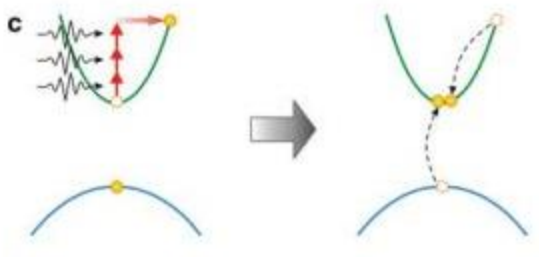

Figure 3.2: Avalanche Ionization [32]

This process is then repeated throughout the presence of the laser field and as a result an exponential increase in the number of conduction-band electrons can be observed, resulting in the formation of a free electron plasma [34]. This mechanism is therefore know as Avalanche ionization and is the dominant ionization process for laser pulse durations that are a few hundred femtoseconds or longer.

3.3 Induced modifications in transparent materials

The energy that has been focused into the substrate, after it has been absorbed by the material via nonlinear absorption, can lead to numerous structural changes that can be observed inside the transparent material at the focal point without effecting the surface. The transfer of energy from electrons to the lattice takes picooseconds after the irradiation and a microsecond timescale is required for thermal energy to transfer out of the focal volume [35].

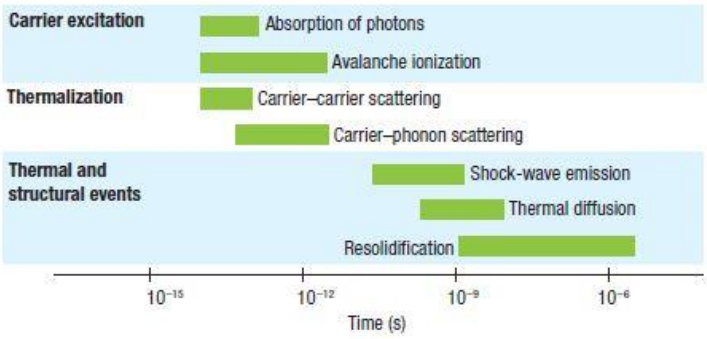

Figure 3.3 : Timescale of laser-matter interaction [35]

Ultrashort pulse irradiation creates a non-equilibrium situation in which a hot and dense free electron plasma is created inside a cold lattice. This minimises thermal diffusion out of the focal volume during the pulse and enables efficient energy deposition. This, in turns, minimises the amount of energy required to modify the material. After the pulse, this free electron plasma then starts cooling down by transferring energy to the surrounding atomic structure. When the heat finally diffuses out of the focal region, the material cools and re-solidifies, leaving a permanent structural change.

To date, three main types of structural modifications have been reported depending on the pulse energy which are *a smooth refractive index change also known as Type I modification* [35,36], *a birefringent refractive index change* [37,38] and *the formation of void also known as Type II modification* [39,40,41].

3.3.1 Smooth Refractive Index/Type I modification

At **low** pulse energies, slightly above the modification threshold, a smooth variation in the refractive index is observed at the modified region which can be either positive, negative or a combination of both. This smooth change in refractive index is necessary to fabricate optical waveguides. The refractive index change occurs as a result of the energy deposited in the focal volume which results in melting and rapid resolidification of the glass. The magnitude of the induced index change depends on the sample material, the laser parameters and on the Numerical Aperture of the focusing objective.

3.3.2 Birefringent Index Modification

At **intermedate** pulse energies, self-organised nano gratings can be formed within the sample material. In fused silica, these consist of alternating layers of material with slightly increased and decreased density. The structures are oriented perpendicular to both, the polarisation vector and the incident direction of the laser beam and give rise to form birefringence [43]. It is believed considered that these “nanogratings” are the result of interference phenomena that lead to periodic modulations in the electron plasma density and therefore to modulations in the nature of the structural change [44].

3.3.3 Void/Type II modification

At very **high** pulse energies, the lattice itself can be turned into a gas or plasma. The pressure at the irradiated volume can cause a micro-explosion due to which hot melted material is pushed into the cold material that eventually leads to the formation of a void[45].

Figure 3.4 summarises the mechanisms of femtosecond laser matter interaction.

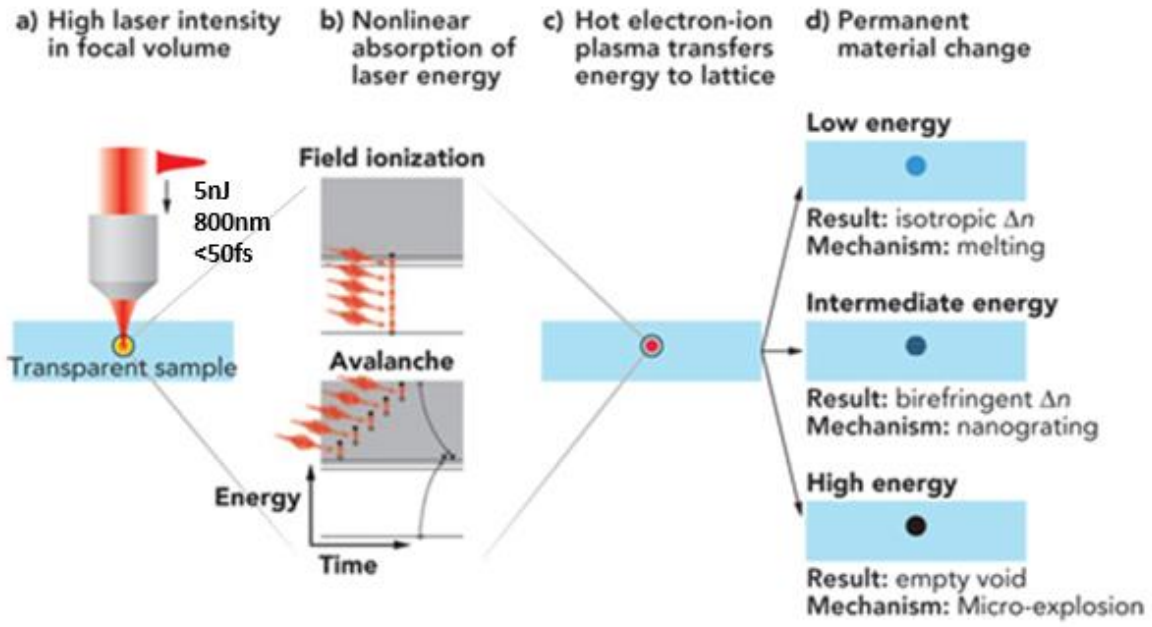

Figure 3.4: Schematic of femtosecond laser-matter interaction processes [68]

3.4 Process parameters for femtosecond-laser direct inscription

The properties and characteristics of inscribed waveguides are strongly dependent on different aspects of the direct inscription process. For example, the ***writing geometry*** is a critical factor. The substrate can move either along or transverse to the direction of propagation of the writing beam and this is therefore known as the Longitudinal or Transverse writing geometry (LWG or TWG) as shown in Figure 3.5. The arrow in the diagram shows the motion direction of the translation stage on which the sample is mounted. Both of these geometries have their advantages and disadvantages. LWG is best for the inscription of circular waveguides, but the structures are limited in length by the working distance of the objective used [46]. In contrast, with TWG long and arbitrary structures can be inscribed efficiently.

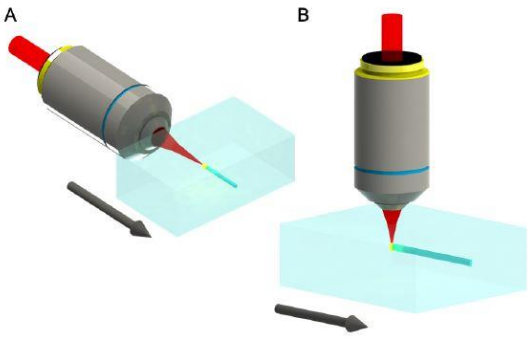

Figure 3.5: (A) Longitudinal writing geometry, (B) Transverse writing Geometry [47]

The used ***focusing optics*** is a crucial aspect to consider as it defines the electric field distribution in and out of the focal region and hence the distribution of the free electron plasma[48]. The dimensions of the formed plasma are directly proportional to the confocal parameter 'b' and beam waist diameter 'D'

$$b = \frac{2\pi n \omega^2}{\lambda}$$

$$D = 2\omega = \frac{2\lambda}{\pi\, NA}$$

where, n is the refractive index of the substrate at the laser wavelength, ω is the beam waist radius, λ is the wavelength and NA is the numerical aperture of the focusing lens [34].The diameter of structures inscribed by LWG are only dependent on the focused beam diameter whereas TWG structures depend on both the confocal parameter and the beam waist diameter inside the material. Furthermore, the ***laser wavelength*** is also a very important factor to consider as direct-inscription relies on nonlinear absorption of light at the laser wavelength and the key parameter in this respect is the number of photons that are required to overcome the bandgap of the sample. Likewise, the ***Pulse Repetition Frequency (PRF)*** is crucial because of its role in thermal accumulation. It was shown that the heat requires ≈ 1.0 µs to diffuse out of the focal region [49]. The size of the written structures thus highly depends on the PRF. Additionally, the ***Pulse Energy*** determines the maximum energy content of the free electron plasma. It therefore also influences the size of the inscribed structure i.e the higher the pulse energy, the larger the size of the structures will be in general. Similarly, the ***translation velocity of sample*** can be used to adjust the total laser fluence on the substrate which can be used to control the size of the laser affected area and thus also the size of the guided optical mode [50].

3.5 Gallium Lanthanum Sulphide (GLS) glass

For the successful realisation of a mid-IR hybrid chip/fibre coupler, the transparency window of the sample material is the most crucial factor for the selection of a suitable material. Other important properties to consider include low losses, few impurities, and high stability to thermal and mechanical stress. Based on these considerations, possible candidates are chalcogenide glasses such as As_2Se_3 or As_2S_3 with a transparency window from 2 - 16 µm, tellurium or germanium based glasses which are transparent up to 20 µm and also silver-halides and zinc selenides with similar ranges of transparency window [51]. For this project, Gallium Lanthanum Sulphide was chosen.

Gallium Lanthanum Sulphide glass (GLS) belongs to the class of chalcogenide glasses which were first studied almost half a century ago but interest into these glasses has increased within the last ten years due to their unique properties for photonic devices. The elements of group sixteen in the periodic table are known as chalcogens. Oxygen exists in this group too but oxygen is not considered as a chalcogen element.

Chalcogenide glasses are composed of two or more components among which, one is usually a chalcogen element such as Sulphur, Selenium, and Tellurium and elements from group III to V of the periodic table [52].

3.5.1 Formation and Purification of GLS

The glass forming ability of Gallium Sulphide and Lanthanum Sulphide was discovered by Loireau-Lozac'h et al. in 1976 [70]. The class of glasses consisting of Gallium Sulphide and Lanthanum Sulphide are named as GLS. The main composition is 70 Ga_2S_3:30 La_2S_3 but this can be modified and adjusted to achieve the desired optical and physical properties. For example, to make a glassy state of Ga-La-S, 2% by weight of Lanthanum oxide is added to help the formation of glass. In order to decrease the possibility of crystallisation and to stabilise the glass network, the addition of oxides is important [53]. The purification of the glass is of utmost importance for scientific and practical work. As impurities even at a very small scale like few parts per million cannot only change the spectroscopic behaviour of a glass, but also result in the loss of power through absorption and scattering. GLS is an inorganic material and takes a deep orange colour. It has a high refractive index, for instance its 2.2880 at 2.9 µm wavelength, and a transmission window that starts from visible and extends up to 10 micron (0.5 to 10 µm). The ultrafast laser inscription process typically

induces a positive refractive index contrast which is essential for the fabrication of waveguides and couplers and GLS is also a non-toxic glass unlike arsenic-based glasses [54]. Additionally, it has a low phonon energy of approximately 450 cm^{-1} [53], and its high nonlinearity and high photosensitivity [53,54] also make it a promising candidate for photonic devices. GLS can exist in both glassy and crystalline states.

The glass is commercially available and the sample for this project was purchased from ChG Southampton Ltd (UK). According to the specifications provided by the company, the elements Lanthanum (III) Sulphide and Gallium (III) Sulphide 70 Ga_2S_3:30 La_2S_3 in powdered form are melted in an atmosphere of Argon gas at 1150 ^{0}C for 24 hours and cooled down rapidly at 20 K/min to avoid crystallization. To increase the stability, the sample is annealed at 500^{o}C for 6 hours and finally cut into glass chips of various sizes [54]. The values of various temperatures for this glass such as melting point, glass transition temperature and crystalline temperature are reported to be 842 ^{0}C, 560 ^{0}C and 720 ^{0}C respectively. Also, the specific density is 4.04 g/cm^2 [54]. The initial sample used in this work was purchased from the company almost 5 years ago (for details see chapter 4) and the sample that was used to fabricate the new chip was purchased from the same company only very recently. The development of an improved purification system by ChG Southampton means that impurity trace level are now less compared to the previous chip. The linear transmission spectra for both these chips will be characterised during the extension of the work in the framework of a PhD project. A high performance spectrophotometer (Agilent Cary 5000) that has recently being installed at Macquarie University will be used for this task.

3.6 Directional coupler design

A directional coupler typically consists of two waveguides that are closely spaced to allow the periodic transfer of energy between the waveguides through evanescent coupling [32]. It's an important building block for various optical circuits such as sensors, power splitters and wavelength multiplexers. A directional coupler has the advantage over a y-splitter (y splitter has only one input port and then at one point which is called branching point it divides into two or more branches and splits the injected light signal) that it avoids radiation loss at the branching point, but its coupling ratio is normally high wavelength dependent. For this project this is not a disadvantage but rather a plus as we eventually want to use the coupler in a ring laser architecture were coupling at the signal wavelength but not at the pump wavelength is required.

The first femtosecond laser written directional coupler was demonstrated by Streltsov and Borrelli [57]. A 2 x 2 directional coupler is fabricated in this work. The shape of the coupler and its working mechanism is shown in Figure 3.6. I_1 and I_2 are input ports and $P_1$and P_2 are the output ports. This device consists of two straight waveguides and subsequent s-bends to bring the waveguides closer to each other. 's' is the core-to-core separation of the waveguides and 'L' is the interaction length. Internal losses in such devices are caused by propagation losses in the waveguides as well as by bend losses. A detailed explanation about individual loss mechanism is given in Chapter 4 (Section 4.1.4).

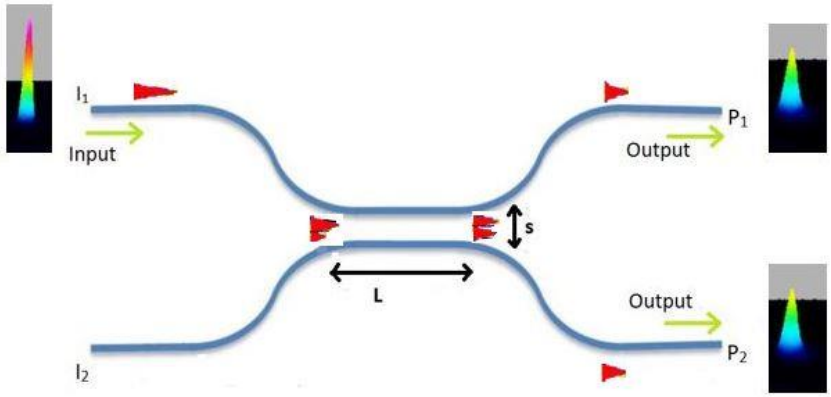

Figure 3.6: Design of a 2 x 2 Coupler

The light guided in the waveguide has a Gaussian-like profile as shown in the diagram and the input signal is coupled into two output ports. The coupling ratio between the waveguides depends on the values of interaction length 'L' and core-to-core separation 's'. Directional couplers are very sensitive to deviations in the writing conditions due to the exponentially decaying evanescent field responsible for the power exchange between adjacent waveguides. These couplers can be used as Wavelength Division Multiplexers (WDMs) which can further be used to realise a ring laser cavity.

4

Design, fabrication and characterisation of a fibre-pigtailed coupler for the mid-IR

The aim to design and demonstrate a fibre-pigtailed 4-port coupler in a mid-infrared compatible glass (Gallium Lanthanum Sulphide) is an important step towards the development of a monolithic guided wave laser cavity which could improve the robustness and compactness of current mid-IR fibre laser systems and lead to an increased efficiency and decreased cavity losses. In general, laser systems that do not rely on any free-space components are usually easy and simple to use by any untrained users as handling does not require alignments or careful operations. Successful low-loss integrated photonic couplers/splitters in mid-IR range can also become the basic unit of fibre ring laser cavities which can further be expanded to enable the generation of ultrashort laser pulses. In this chapter, all the initial steps and experimental measurements have been explained which helped to design and then fabricate a low loss coupler. Also, a procedure to characterise the fabricated

waveguides at a wavelength of 2.9 µm and 1.15 µm, respectively, is discussed. At the end, a conclusion is summarised.

4.1 Characterisation of an existing chip

As an initial steps of this project it was necessary to estimate the fabrication parameters required to design and femtosecond laser-inscribe a single-mode, low-loss coupler into GLS glass. The ability to fabricate single-mode waveguides is essential to minimise the mode mismatch losses as the fibres further used in the experiment for injecting and collecting light to/from the coupler are single-mode fibres. As a starting point for these investigations, an existing chip that was fabricated in the framework of an astro-photonics project by a PhD candidate at Macquarie University, (Mr. Thomas Gretzinger) was characterised. This chip was initially designed and written to operate at a wavelength of 4 µm and therefore a thorough characterization of its performance at 2.9 µm was crucial to obtain important information about the fabrication parameters that would result in low loss couplers for fibre lasers operating around 3 µm. This chip was fabricated by using the setup for ultrafast fabrication available at Macquarie University. Schematic diagram of the setup is shown in Figure 4.1.

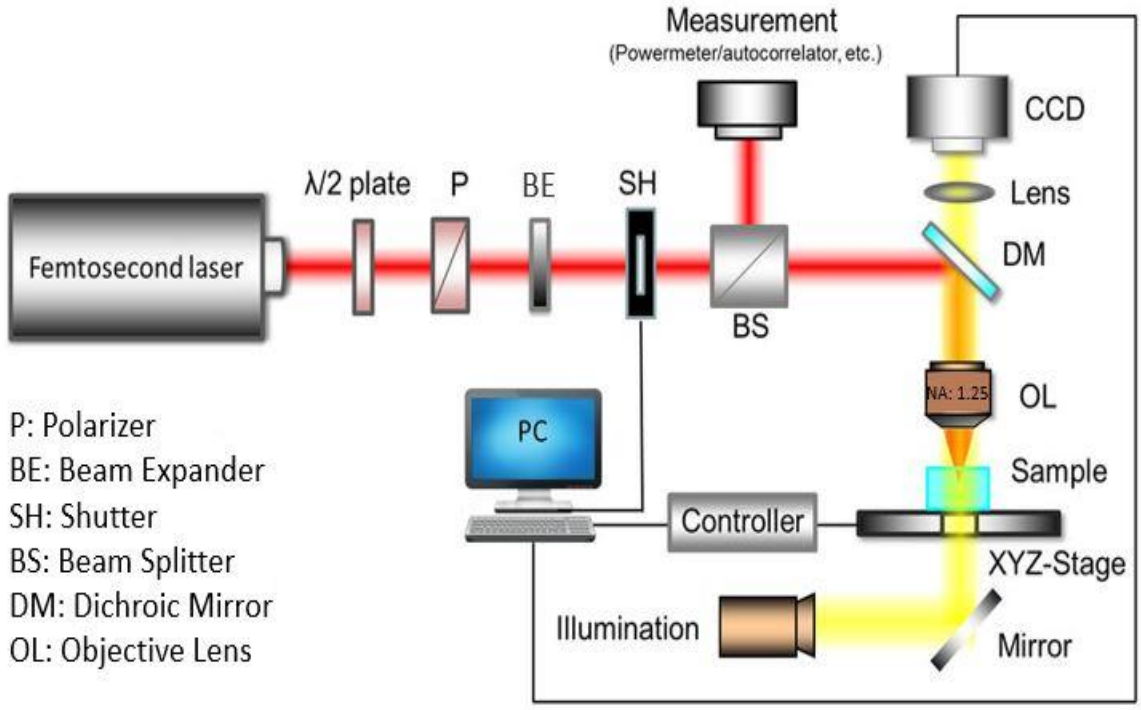

Figure 4.1: Schematic of the setup for femtosecond laser inscription [69]

The energy of the (linearly polarized) laser pulses that are emitted by a femtosecond laser is first adjusted by the combination of a rotatable λ/2-plate and a linear polarizer. Furthermore, a 1:2 beam expander ensures the uniform illumination of a microscope objective as shown in the Figure 4.1. Finally, after passing through a beam splitter and shutter, the light is focused into the sample using a microscope objective. The sample is being mounted on a set of computer controlled Aerotech air-bearing translation stages to move the sample in three dimensions. A photograph of the setup available at Macquarie University is shown in Figure 4.2. The same setup that was used for the fabrication of initial chip by Gretzinger was also used for the fabrication of a new chip as will be explained later.

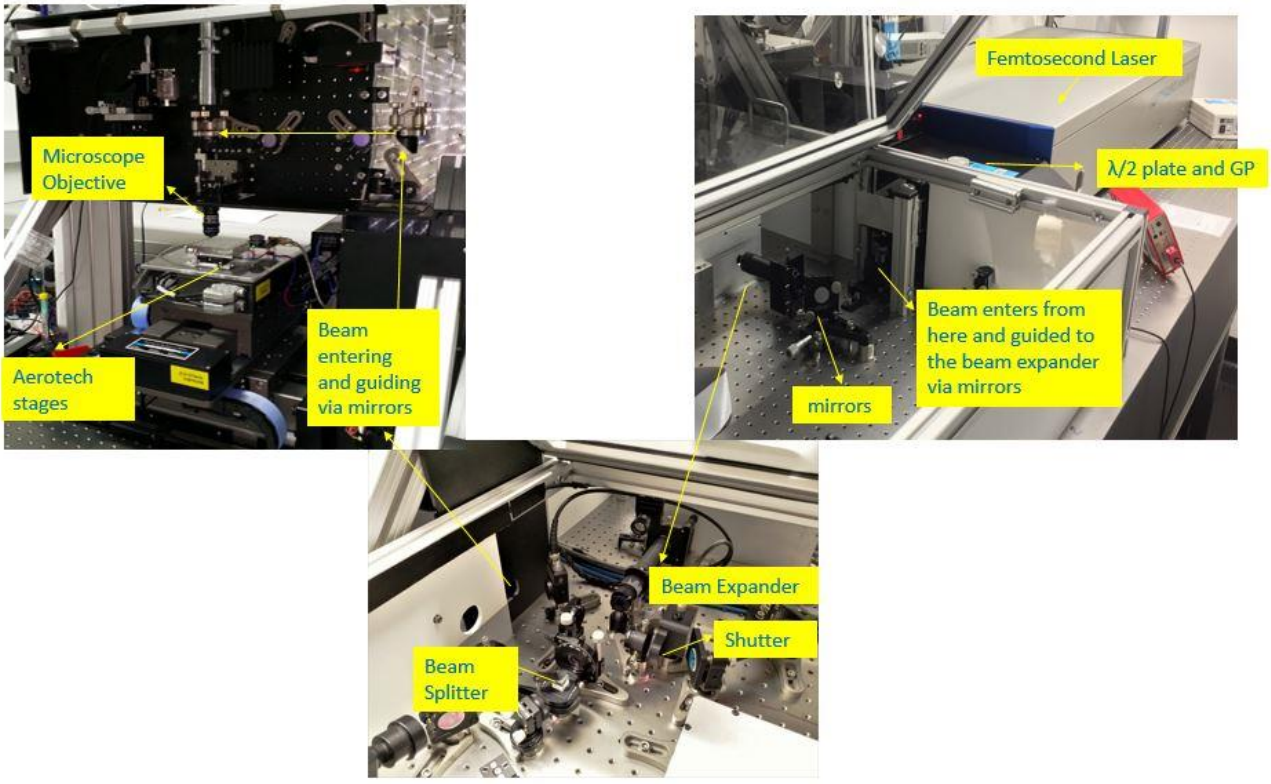

Figure 4.2: Photographs representing the setup of femtosecond laser inscription

The exact parameters that were used for fabricating the initial chip were as follows: The laser source was a 5.1 MHz Ti:sapphire chirped pulse femtosecond oscillator (Femtosource XL 500,Femtolasers GmbH) which emits a train of pulses with a maximum energy of 550nJ and a pulse duration of < 50fs at a wavelength of 800 nm [58]. The sample was translated at a speed of 100 mm/min. The microscope objective used had a Numerical Aperture (NA) of 1.25 with 100× magnification. An oil immersion objective was used to reduce the spherical aberrations due to the refractive index

mismatch. The waveguides were fabricated at a depth of 180 µm below the top surface. Mr. Gretzinger is acknowledged for providing this photonic chip for the initial steps of this project.

The dimensions of the chip were 12.65 × 10.34 × 1.06 mm which were measured using a Vernier calliper. The chip contained single-tracks of waveguides that were written at different pulse energies ranging from 7nJ - 14nJ and then a series of double-tracks that were inscribed at 11 nJ energy with a range of centre to centre distance as shown in Figure 4.3 (a & b). The femtosecond laser fabrication process in GLS produces a positive refractive index change and a tear-drop shaped refractive index profile, as shown in Figure 4.3 (a), which leads to a highly elliptical beam profiles [59]. In order to ensure a circular confined mode, six double scans at the same energy 11 nJ but with a varying centre-to-centre separation of 5.6 µm, 6.3 µm, 7 µm, 7.7 µm, 8.4 µm and 9.1 µm were inscribed as shown in Figure 4.3 (b).

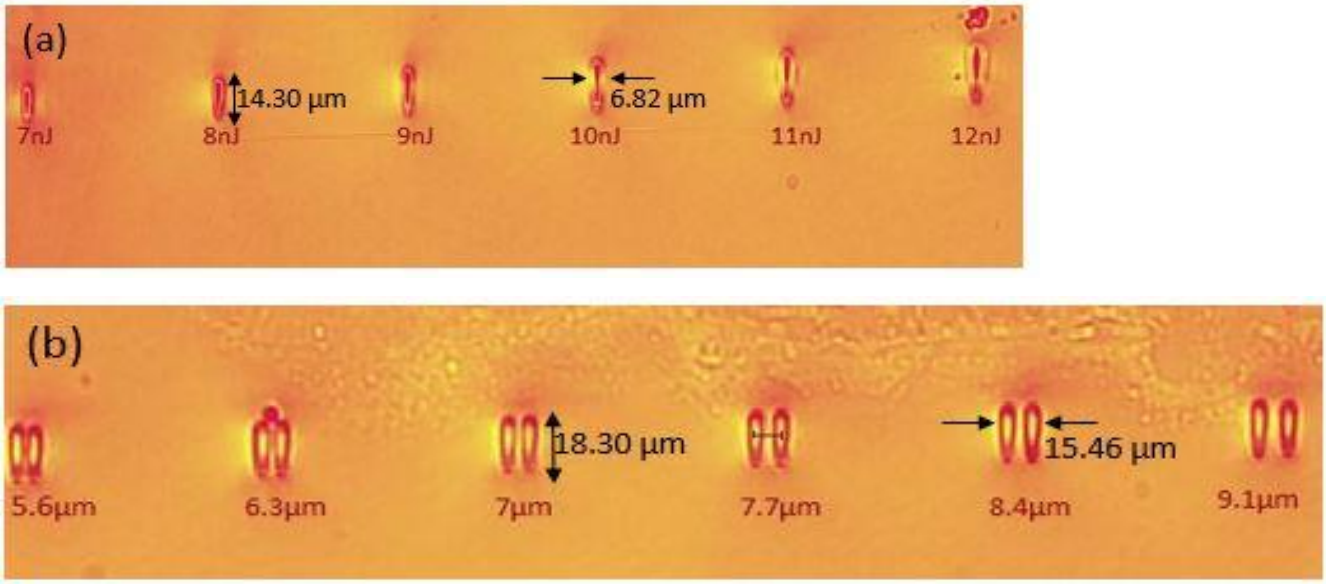

Figure 4.3 (a) Six single track waveguides fabricated at different laser pulse energies (b) Six double tracks with varying core to core separation distance

It can be seen from Figure 4.3 (a) that an incremental increase in laser energy increases the sizes of the written waveguides in both x and y direction. The chip was first inspected under an optical microscope in transmission mode and the dimensions along x and y direction of the single track and double track waveguides were recorded as shown in Table 4.1.

Number of single track Waveguides	Laser Pulse Energy (nJ) (Fabrication)	Height of the waveguide (µm)	Width of the Waveguide (µm)
1	7	12.80	4.99
2	8	14.30	5.49
3	9	15.96	6.32
4	10	16.96	6.82
5	11	18.30	7.48
6	12	19.95	7.31
7	13	21.94	8.48
8	14	22.78	8.81

Number of double track Waveguides	Laser Pulse Energy (nJ) (Fabrication)	Core-to-core Separation (µm)	Height of the waveguide (µm)	Width of the waveguide (µm)
1	11	5.6	18.30	12.63
2	11	6.3	18.30	13.43
3	11	7	18.30	14.10
4	11	7.7	18.30	14.83
5	11	8.4	18.30	15.46
6	11	9.1	18.30	15.89

Table 4.1: Dimensions of the fabricated waveguides

4.1.1 Characterisation Setup

The setup used for the characterisation and mode profile analysis is explained in this section. In order to produce an output signal of 2.9 µm from a $Ho^{3+:}$ Pr^{3+} co-doped ZBLAN Fibre, 1.15 µm pump photons are required to excite the electrons to the required transition levels as explained in Section (2.4.1). An Eagleyard Photonics high power diode laser at 1.15 µm is available in the lab to couple into the inner cladding of a double-clad $Ho^{3+:}$ Pr^{3+} co-doped ZBLAN fibre using a 20 mm focal length uncoated Ca_2F lens with a coupling efficiency of 73% (Figure 4.5 Right). The input and output ends of the fibre were cleaved perpendicularly to the fibre axis. The output end of the fibre emitted a 2.9 µm wavelength light signal which is further launched in to the optical chip via butt-coupling. In butt-coupling, the tip of the fibre is placed very close to the input facet of the waveguide while ensuring that it is not touching the chip to avoid damage. For this project an optical microscope was mounted at the top of the chip which is shown in Figure 4.5 (Left) to keep checking while butt-coupling. The recorded image of this microscope is shown in the figure 4.6. The resulting air-glass interfaces set up a Fabry-Perot cavity that provide the necessary feedback for the fibre laser cavity. After the light has been propagated through the waveguides inside the chip, the output facet of the waveguide chip is imaged by a 20 mm CaF_2 lens on to an imaging Camera (CCD mid-IR camera) to observe the transmitted spatial mode structure. The pump signal (1.15 µm) is blocked by a pump filter that is transmitting light only in a wavelength range 2.4 - 4.6 µm hence blocks 1.15 µm pump signal. Figures 4.4 and 4.5 represents the schematic setup diagram and the actual lab setup used for the characterisation.

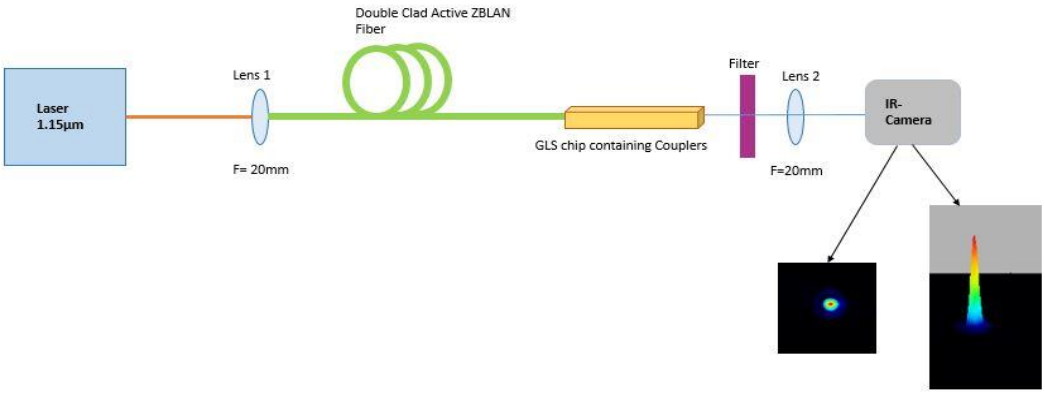

Figure 4.4: A schematic of the characterisation Setup

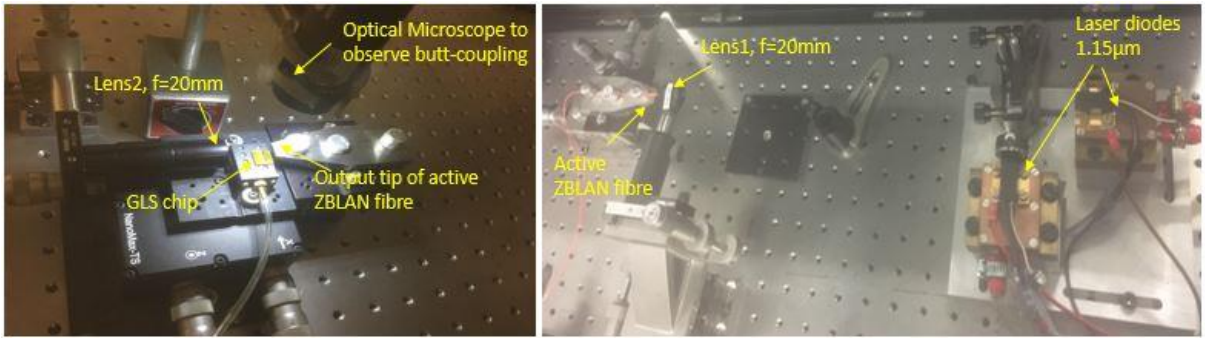

Figure 4.5: (Right) Laser diodes (1.15 µm) coupled to Active ZBLAN Fibre via lens, (Left) Light signal (2.9µm) from the fibre tip butt-coupled to the GLS chip and waveguide output focused on Lens to see the image on IR-Camera.

High-resolution 3-axis manual positioners (Nanomax MAX313D, Thorlabs) were used for coupling light in and out of the chip. A microscope which is mentioned earlier being used for butt-coupling can be seen in the bottom right picture of figure 4.5. This microscope also helps to find the waveguide tracks as shown in Figure 4.6.

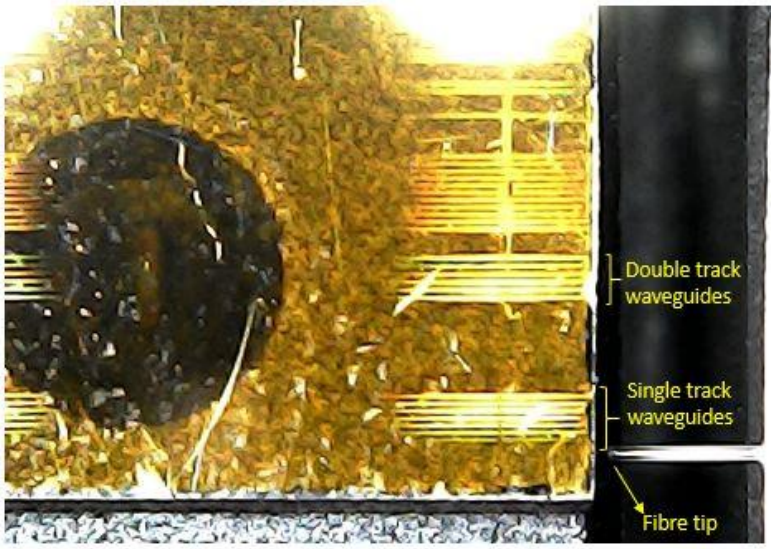

Figure 4.6: Fibre tip injecting light into the single tracks fabricated in the GLS chip

4.1.2 Mode Profile Analysis

As a next step, the mode nature of the waveguides is determined by injecting light with a wavelength of 2.9 µm into the individual waveguides. Firstly, the light is launched into the centre of the waveguide to excite the fundamental mode. To confirm whether the waveguide also supports higher order modes, the launch conditions of the input light signal were subsequently changed. The input focal plane was shifted to an off-axis position along both, x and y directions, and the change in the output mode profile is observed on the camera image. If the light remains confined to the fundamental mode (and only changes in intensity) and doesn't change into other shapes (compare the mode profiles shown in figure 2.4) it can be concluded that the waveguide is single-moded otherwise it is multi-moded.

The images recorded for the 8th single track waveguide, fabricated at 14 nJ are shown in Figure 4.4. The left image shows the fundamental mode when light is injected exactly into the centre of the waveguide whereas the right image shows the excitation of higher-order modes when light was injected off-axis along the y-direction, i.e this waveguide is not single-moded.

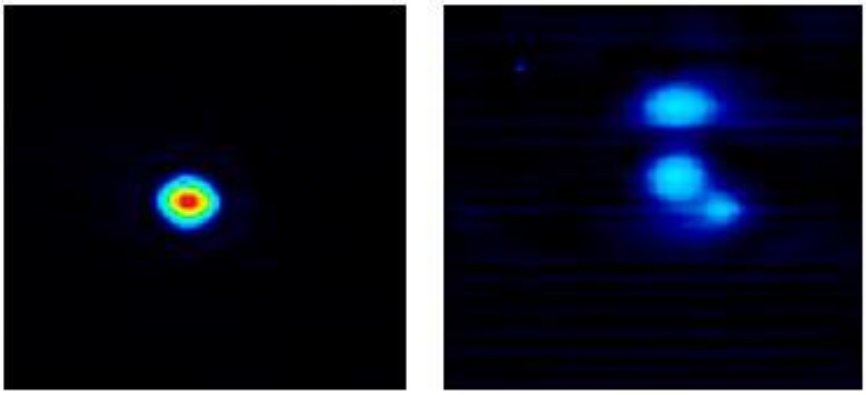

Figure 4.7: (Left side) Fundamental mode of the waveguide, (Right side) Off-axis image representing the multimode nature of the 8th single track waveguide.

In single tracks, the mode behaviour is examined along both x and directions. The first six single track waveguides are found to be single-mode, the 7th is in a transition state (borderline of becoming multi-mode) and the 8th waveguide is clearly multimode. This is summarised in Figure 4.8. All the double track waveguides were fabricated at a pulse energy of 11 nJ. At this energy, single track waveguides are single-moded but in double tracks waveguides, a careful examination is required for multimode behaviour off-axis along the x-direction. Although the height of the waveguides remains the same for the double track waveguides compared to a single trach waveguide inscribed at 11 nJ, the dimensions along the x-plane are increasing proportional to the core-to-core separation of the double tracks. A careful analysis revealed that the first five double tracks are single-moded while the 6th one is behaving in a transition mode. A summary of the mode-behaviour of the individual waveguides is presented in Figures 4.8 and 4.9 below.

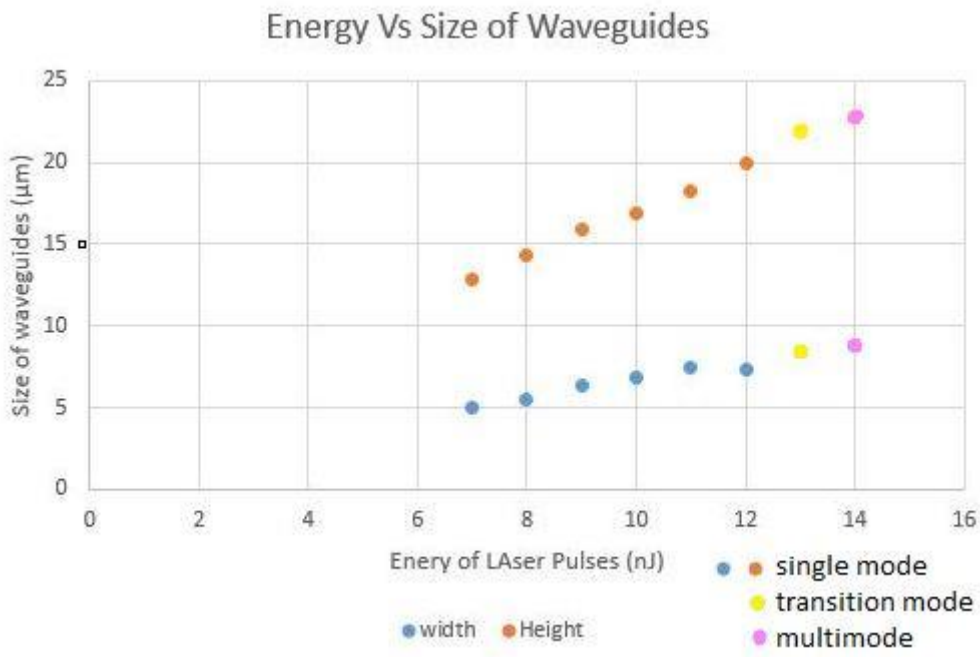

Figure 4.8: Mode Nature of single track waveguides fabricated at energies 7nJ to 14nJ

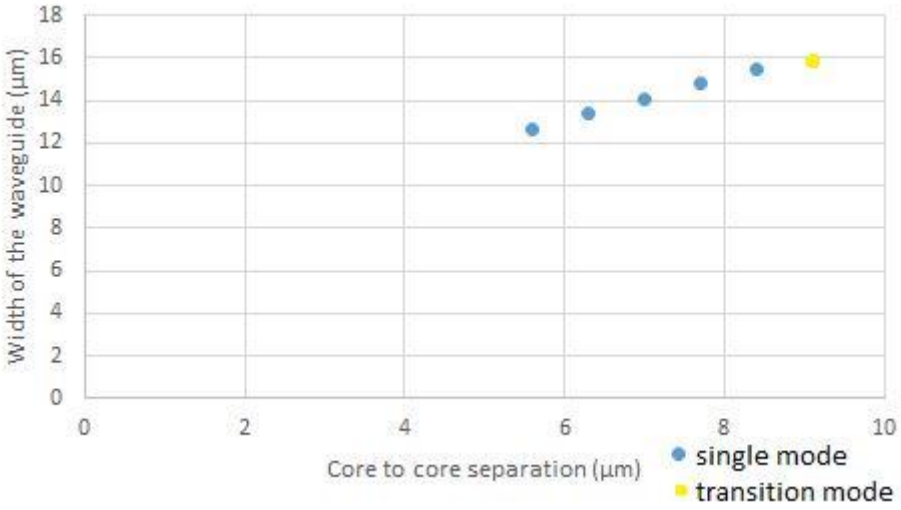

Figure 4.9: Mode Nature of double track waveguides

As a next step, the insertion loss of the individual waveguides in the existing chip were investigated.

4.1.3 Characterization of single and double track waveguides

When a light signal is coupled into the waveguides, it experiences losses at the interface and inside the chip. The different types of losses are explained in the next section.

4.1.4 Insertion Loss

The insertion loss is the total reduction in light intensity when passing through a waveguide in an optical chip. This loss is the result of four factors; Fresnel Reflection Loss, Input coupling loss, propagation loss and bend loss.

Insertion loss (dB) = Fresnel Reflection loss + Input Coupling loss (dB) + Propagation loss (dB) + Bend loss (dB)

(i) Fresnel Reflection loss occurs at the input and output interface of the chip. At one face, its value can be calculated using the equation

$$Fresnel\ Reflection\ Loss = 10\ log\left[1 - \left(\frac{n_{glass} - n_{air}}{n_{glass} + n_{air}}\right)^2\right], \qquad (4.1)$$

where n_{glass} is the refractive index of the glass (GLS) chip and n_{air} is the refractive index of the air. The value of n_{air} is approximately 1 and the value of n_{glass} at 2.9 μm is 2.2880 [54]. Fresnel Reflection loss at one interface as calculated using above formula is 0.72 dB and it will be doubled for both faces so the overall Fresnel reflection loss is 1.44 dB for 2.9 μm light.

(ii) The second type of loss mentioned above is input coupling loss. It is because of two different losses.

(a) Numerical Aperture (NA) mismatch loss

(b) Mode Field Diameter (MFD) mismatch loss

To measure the NA of the fabricated waveguides, Marcuse Formula can be used

$$\frac{w}{a} \approx 0.65 + \frac{1.619}{V^{3/2}} + \frac{2.879}{V^6}, \qquad (4.2)$$

where 'w' is radius of the fundamental mode supported by the waveguide and 'a' is the actual radius of the waveguide as measured under the microscope. This formula was used for the calculation of the V number of the waveguides, and then the NA was calculated using equation 2.1. And after calculating the NA of the fabricated waveguide and by knowing the NA of the fibres used in these experiments (the $Ho^{3+:}$ Pr^{3+} co-doped ZBLAN Fibre has an NA of 0.13), the NA mismatch loss in dB can be calculated by the equation.

$$NA\ mismatch\ Loss\ (dB) = 10 \log\left(\frac{NA_2}{NA_1}\right)^2, \qquad (4.3)$$

where NA_2 is the Numerical Aperture of the fibre which is launching the light into the waveguide and NA_1 is the Numerical Aperture of the waveguides itself ($NA_1 < NA_2$).

The calculated NA values of the double track waveguides using above formulas range between 0.112 - 0.137 and therefore using equation (4.3), the calculated NA mismatch loss is less than 1dB in all cases.

Once the NA of the waveguide is calculated, the refractive index change of the fabricated waveguide can be calculated using equation

$$NA = \sqrt{{n_{core}}^2 - {n_{clad}}^2} \qquad (4.4)$$

For this case, n_{core} is the refractive index of the waveguide and n_{clad} is the refractive index of the bulk GLS and it is n_{clad} = 2.2880 [54]. $\Delta n = (n_{core} - n_{clad})$ can be used to calculate the change in refractive index. The calculated Δn values are ranging from $3.69 \times 10^{-3} – 4.9 \times 10^{-3}$.

To measure the Mode Field Diameter mismatch Loss, the following equation can be used:

$$Mode\ Field\ Diameter\ Mismatch\ Loss = 10 \log\left(\frac{4}{\left(\frac{MFD\ 1}{MFD\ 2} + \frac{MFD2}{MFD1}\right)^2} \right), \qquad (4.5)$$

where, “MFD 1” is the Mode Field Diameter of the core of the fibre and “MFD 2” is the Mode Field Diameter of the mode propagating through the waveguide.

(iii) Another loss mentioned earlier is propagation loss. As the light propagates through the waveguide, some of its energy is lost due to scattering, absorption and coupling into radiation modes. This loss depends on the wavelength of the light signal, the material of propagation and the properties of the waveguides.

(iv) Also, in the design of coupler shown in the figure 3.6, losses due to the s-bends are potentially present as well. A formula for the curvature loss was introduced by Marcuse[60] which can be can be used to calculate the minimum bend radius required for these s-bends to be negligible. For our design, all bend radii are well above this minimum value and therefore bend losses do not need to be included in this work.

The input coupling loss depends on Mode Field Diameter (MFD) mismatch and Numerical Aperture (NA) mismatch. The MFD and NA of the fibres used are known from the manufacturers whereas the MFD and NA of the fabricated waveguides can be measured and calculated by equations (4.3, 4.4 and 4.5), respectively. The MFD and NA of the fabricated waveguides depend on the femtosecond

laser inscription parameters as described in Chapter 3. To decrease the input coupling losses, a careful selection of fabrication parameters is required.

4.1.5 Measuring the Insertion Loss

The total Insertion Loss is measured for the fabricated single tracks and double track waveguides, using the characterization setup shown in Figure 4.4. A Matlab code is written to integrate the mode profile which is recorded by the CCD camera. The integration of the mode profile is proportional to the power of the laser beam (P_{in}) injected into the waveguide and also the power coming out of the waveguide (P_{out}) and the loss is thus measured using the equation,

$$Loss = 10 \log\left(\frac{P_{out}}{P_{in}}\right), \quad (4.6)$$

where P_{out} is the output power from the waveguide and P_{in} is the input power given to the waveguide. The results are mentioned in Table 4.2. These values are measured as accurate as possible but still there is a possibility of slight errors in the values. The margin of error in the measurement of dimensions of the waveguides is ±0.8 µm and in the propagation loss it is ±0.07 dB/cm.

Single Track Waveguide	Laser Pulse Energy (nJ) (Fabrication)	Total Insertion Loss (dB)
1	7	9.27
2	8	6.33
3	9	6.52
4	10	5.87
5	11	4.86
6	12	5.55
7	13	4.90
8	14	5.06

Double track waveguides	Laser Pulse Energy (nJ) (Fabrication)	Core-to-core Separation (µm)	Total Insertion Loss (dB)
1	11	5.6	4.66
2	11	6.3	5.71
3	11	7	5.23
4	11	7.7	5.65
5	11	8.4	4.60
6	11	9.1	3.20

Table 4.2: Total insertion loss of single and double tracks waveguides

After measuring the total insertion loss; the NA mismatch Loss, Mode Field Diameter mismatch loss and change in refractive index (Δn) is calculated using the above-mentioned procedure. After this, the propagation loss for each waveguide can be calculated by using the equation

Propagation Loss = Total Insertion Loss – (NA mismatch loss + MFD mismatch Loss + Fresnel reflection Loss) (4.7)

The values of NA mismatch loss, change in refractive index (Δn), Mode Field Diameter (MFD) Mismatch Loss, Fresnel Reflection Loss at both interfaces of the chip and the Propagation Loss is calculated for the double tracks using above equations. These results for a double track waveguide is summarised in Table 4.3.

Various Losses	Loss in dB
NA mismatch Loss	0.01
MFD mismatch Loss	0.14
Fresnel Reflection Loss	1.44
Total Insertion loss	5.23
Propagation Loss /1.26cm	3.65
Propagation Loss/cm	2.89

Table 4.3: Measured and calculated losses of the testing chip

The characterization and the calculation of losses paved the way to fabricate a low loss coupler.

4.2 Fabrication of integrated couplers for mid-IR fibre lasers

The above-mentioned results provided the basis for the fabrication of directional couplers in a new GLS glass chip that was purchased from ChG Southampton Ltd (UK). The glass had the same composition as compared to the previous chip but improved purification and manufacturing methods resulted in reduced levels of impurities. The couplers were inscribed into the new chip using the same fabrication setup as shown in Figure 4.1 and 4.2. The aim was to fabricate a fibre-pigtailed mid-IR low loss, single-mode, wavelength-selective Directional Coupler (DC) for an integrated Ho-Pr fibre laser. While in the previous chip, double tracks were inscribed (compare Figure 4.2(b)), for the fabrication of couplers in the new chip the inscription of triple tracks was chosen in order to better match the height and width values of the resulting waveguides and thus to make the waveguide mode more circular and better matched to the core of the fibre (core diameter of the fibre = 13 μm). This was thought to further reduce the Mode Field Diameter Mismatch losses. Waveguides were inscribed at a depth of 180 μm below the glass surface with an incident laser pulse energy ranging from 10 nJ to 13 nJ. The dimensions of the GLS chip were 9.57 x 9.97 × 0.99 mm. The details of all the fabricated waveguides and couplers is as follows:

- Triple-tracks straight waveguides were fabricated at 10 nJ, 11 nJ, 12 nJ and 13 nJ pulse energy. These energy values were selected on the experience of the previous chip as these were supposed to provide single mode guidance for the 2.9 µm signal. The core-to-core separation values of the three tracks in each waveguide were selected to be 4.2 µm for 10 nJ energy waveguides, 4.55 µm for 11 nJ, 4.9 µm for 12 nJ and 5.25 µm for 12 nJ energy waveguides.
- Four sets of couplers are fabricated using these triple track waveguides written at 10 nJ, 11 nJ, 12 nJ and 13 nJ laser pulse energy, respectively. For instance, the first set consists of triple track waveguides fabricated using 10 nJ energy. Similarly, in the second set all waveguides were fabricated at 11 nJ laser pulse energy and in the third set at 12 nJ. Finally, in the fourth set of couplers all waveguides were inscribed with 13 nJ laser pulse energy. Furthermore, all sets consist of eight couplers each with the first four couplers fabricated with a core-to-core separation of 24 µm and the remaining four with a separation of 26 µm:

  (i) The first four couplers in each set consists of a fixed value of core-to-core separation‘s’ (s = 24 µm) while the interaction length ‘L’ increases from 0 mm to 3 mm with a step size of 1 mm.

  Similarly,

  (ii) The second four couplers in each set consists of a fixed value of core-to-core separation ‘s’ (s = 26 µm) while the interaction length ‘L’ again increases from 0 mm to 3 mm with a step size of 1 mm.

The input-to-input port distance is kept at 125 µm and the bend radius for the s-bends of the coupler is 40 mm. This value of input-to-input port separation was selected keeping in mind the core and cladding diameters of the fibres used. With this distance, fibre butt-coupling at the input or output ports of the coupler was still possible and the bend radius was large enough to that bend losses could be neglected. Further, the length of the chip was kept as short as possible to minimise propagation losses. The design is shown in Figure 4.10.

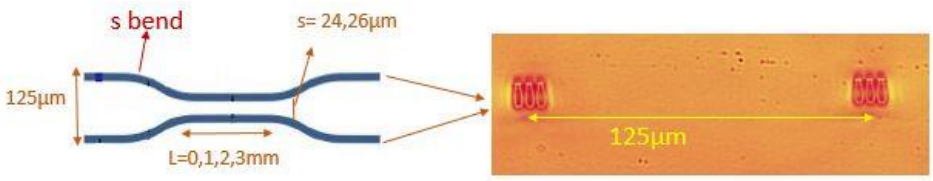

Figure 4.10: A Schematic of a coupler and an optical image of inputs of a coupler

The sample facets were polished after the inscription for an optimum optical quality as due to edge effects during Femtosecond laser inscription the sides of the chips can become unusable [61]. The chip was observed under the microscope to measure the dimensions (width and height of the triple tracks) and the microscopic images of the facets of the triple tracks along with the values of sizes are shown in Figure 4.11.

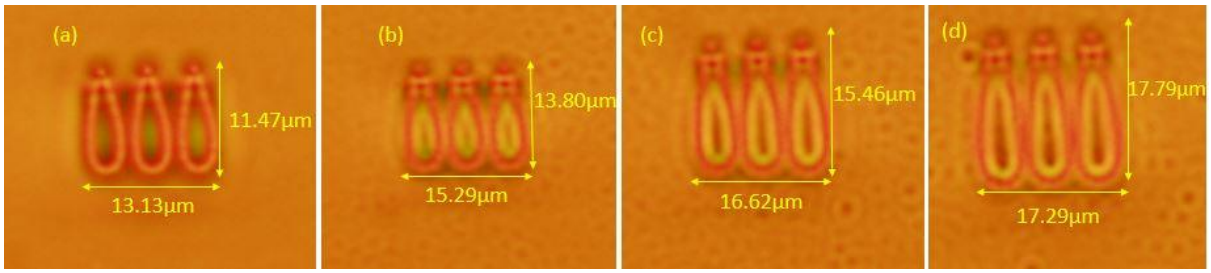

Figure 4.11: Dimensions of the triple tracks fabricated at laser pulse energy (a) 10nJ (b) 11nJ (c) 12nJ and (d) 13nJ

4.3 Mode Profile Analysis

The chip was first analysed to check the mode profile of the triple tracks by injecting the light signal at 2.9 µm wavelength into the waveguides and observing the change in their mode-shape when moving the input focal plane off-axis as explained in detail is Section (4.1.2). It was found that the 10 nJ and 11 nJ energy triple tracks are single-moded at this wavelength while the 12 nJ and 13 nJ energy triple tracks are multi-moded. Thus, for the subsequent characterization, the couplers consisting of waveguides fabricated at 10 nJ and 11 nJ energy were used.

An image of the mode profile is shown in Figure 4.12 (a & b) for the 12nJ energy triple track waveguide and clearly shows the multi-mode nature of the waveguide.

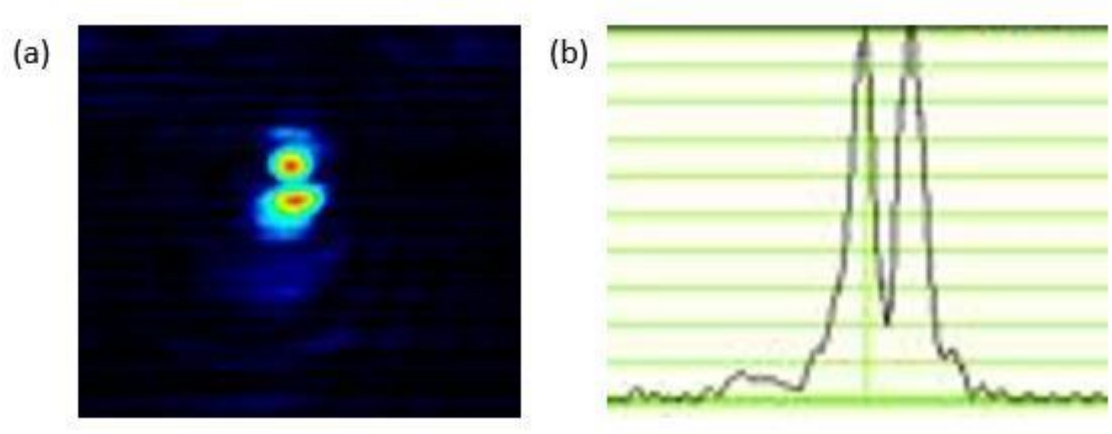

Figure 4.12: Image to represent the multimode nature of the waveguide

4.4 Characterisation of the Couplers

As a next step, the fabricated couplers are characterised using the characterisation setup as shown in Figure 4.4. The input and output power was directly measured using a power meter instead of integrating over the mode profile as was done previously (Section 4.1.1). An iris is used to ensure that only light that is guided in the waveguide is captured and all the background noise is blocked. Images of the output facets of the directional couplers are presented below in Figure 4.13. These images clearly shows the variation in coupling of the injected light signal in different couplers for different coupling region (interaction) lengths.

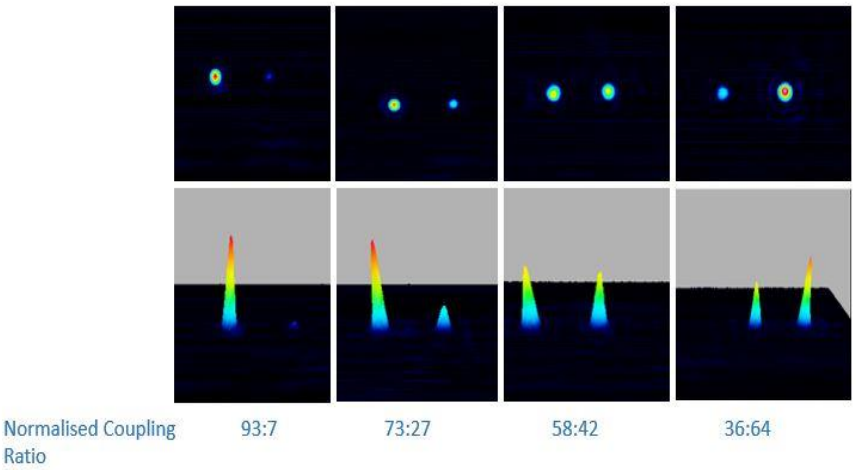

Figure 4:13: Output facets of the directional couplers presenting variation in coupling of light signal as couplers have various interaction length regions

As it is explained in section 4.2, the first eight couplers were fabricated with 10 nJ laser pulse energy and the interaction region varied in length L = 0 - 3 mm with a step size of 1 mm. The separation

between the waveguides was 24 µm in the interaction region for the first four couplers and 26 µm for the last four couplers. The next eight couplers are fabricated at 11 nJ laser pulse energy with the same variation for 'L' and 's'. This information is summarised in Figure 4.14 as well.

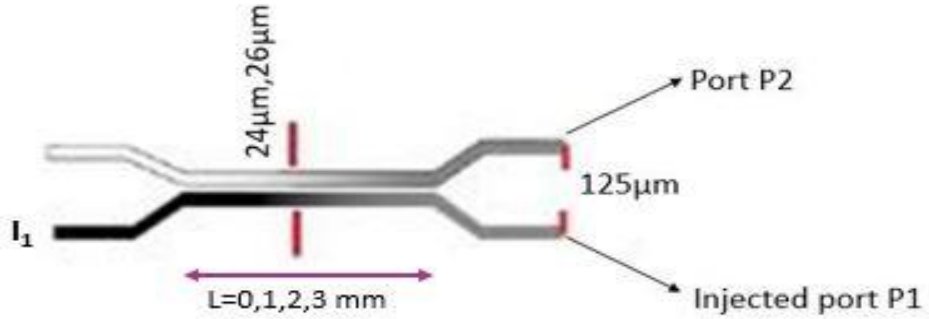

Figure 4.14: A Schematic of a coupler

When the light was launched at one of the input **I_1,** the output is recorded at the output ports P1 and P2. The output port P1 is the output end of the same waveguide of the coupler whose input end was being injected by the light signal therefore names as an injected port P2. The coupling variation was observed due to the change in interaction length and spacing between the waveguides in the interaction region. The graphs (Coupling ratio vs interaction length of the coupling region) were plotted for these couplers. Figure 4.15 and 4.16 summarised this information.

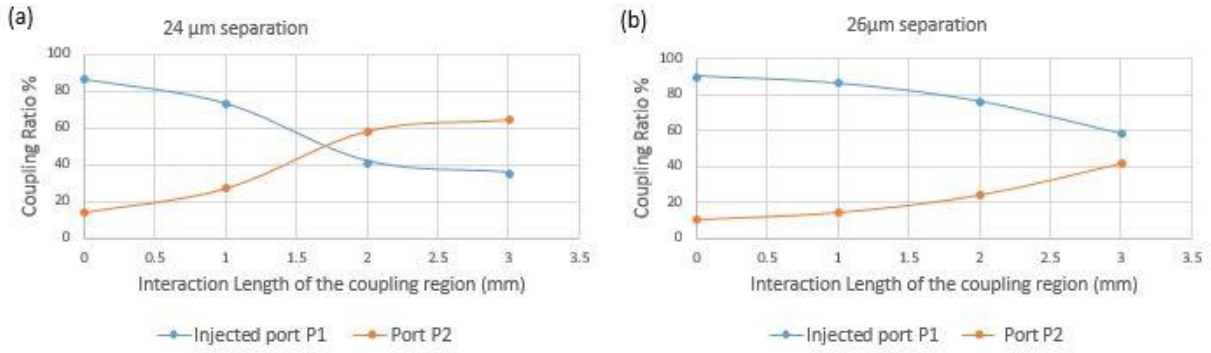

Figure 4.15: Variation in coupling ratio with respect to the length of the coupling region for the couplers fabricated at 10nJ pulse energy having separation 's' of (a) 24µm and (b) 26µm

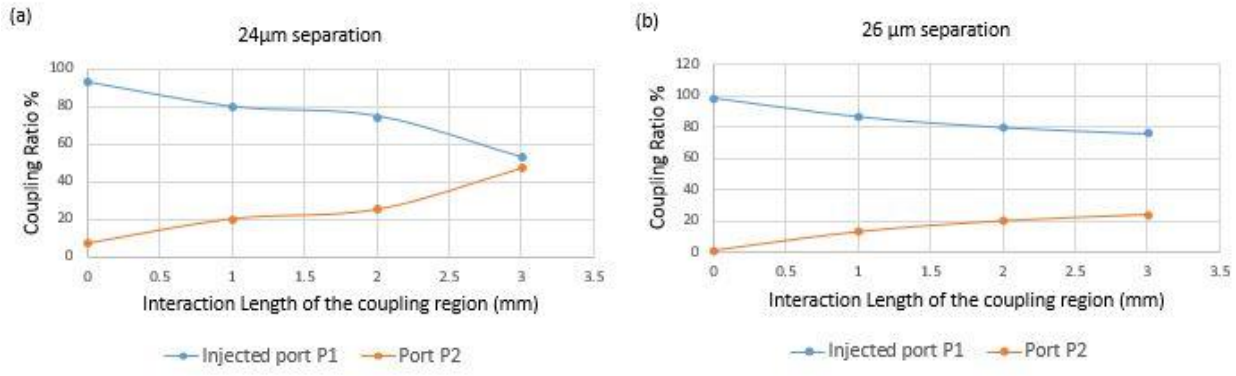

Figure 4.16: Variation in coupling ratio with respect to the length of the coupling region for the couplers fabricated at 11nJ pulse energy having separation 's' of (a) 24µm and (b) 26µm

It can be seen from these graphs that, as the coupling region waveguides separation increases the coupling ratio decreases as expected for evanescent coupling.

The total insertion loss is measured, and the NA mismatch Loss and MFD mismatch loss is calculated for these couplers. A summary is presented in Table 4.4.

Various Losses	Loss in dB
NA mismatch Loss	3.19
MFD mismatch Loss	0.10
Fresnel Reflection Loss	1.44
Total Insertion loss	8.3
Propagation Loss/cm	3.57

Table 4.4: Measured and calculated losses of couplers in GLS chip at 2.9 µm

A comparison of the results calculated for the new chip and the previous chip revealed that the propagation loss/cm has actually increased instead of decreasing. Further investigations are required to find the root cause of this increase. This means that the induced refractive index change in the new chip during fabrication is now actually smaller as compared to the testing chip and also that the propagation loss is higher in the previous chip. At present, the specific mechanisms that lead to a modification of the refractive index in GLS upon femtosecond laser irradiation is poorly understood, which makes it difficult to optimise the inscription process other than via trial-and-error. In future, spatially-resolved Raman Spectroscopy can be used as a tool to investigate the structural changes within the glass network induced by femtosecond laser pulses. Another factor

which can be responsible for the smaller refractive index change and the decrease in the Δn value can be the result of more purified sample. The initial chip used for this project was less purified and the new sample purchased from the ChG Southampton Ltd (UK) is reported to be more pure (having less OH^- and SH^- ions). Although the high purity sample was assumed to give lower losses, the experimental data is not supporting this. More investigation is required to figure out the reason of this increase in loss and a critical optimisation of the fabrication parameters will be required to realise a low-loss fibre pig-tailed GLS chip for a fully-integrated guided-wave laser.

4.5 Fibre-pigtailed coupler

As the aim of the work was to fabricate a fully fibre pigtailed device, the output facets of the coupler were coupled to a passive ZBLAN fibres (core diameter 13µm, cladding diameter 125µm) fibre. As the spacing between the individual input and output ports of the coupler is 125µm, this fibre was selected so that when two of these same fibres were directly joined together, this gives rise a core-to-core separation of 125µm as shown in the figure 4.17(c). As the ZBLAN fibre has a core diameter of 13 µm, cladding diameter of 125 µm and then a polymer coating layer to protect the fibre, to join the fibres as shown in the figure 4.17 is not an easy step. The fibre was first placed in paint stripper to remove the polymer coating so the core and first cladding is exposed. Then, these fibres were placed on a glass slide under the microscope to align them axially as shown in Figure 4.17(b) with the help of a drop of glue. The selection of the glue is also very important and it is based on the refractive index value of the glue. It was specifically selected to have a lower value then the refractive index of the ZBLAN fibre so the coupled signal can be guided and no light lost is lost due to the glue.

Figure 4.17 (a) shows an image of two fibres joined on a glass slide with a glue drop and figure 4.17(b) is the close image of the tips of the fibres aligned axially together and figure 4.17(c) is the cross-section view of the fibre tips.

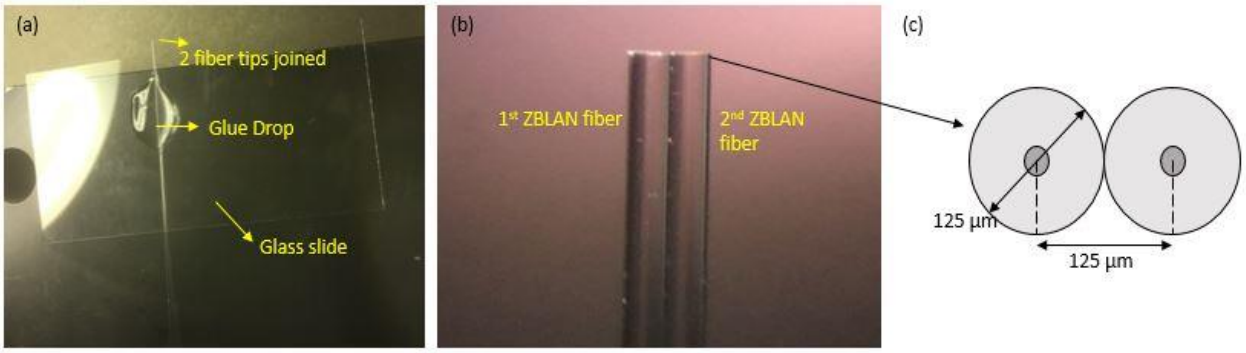

Figure 4.17: Fibre tips joined together

The same setup that was used for the characterization of the couplers is used with some additional stages to place the two joined ZBLAN fibres. The picture of the setup used to get the signal coupled from the output facets of the coupler into the two joined fibres is shown below in figure 4.18(a and b).

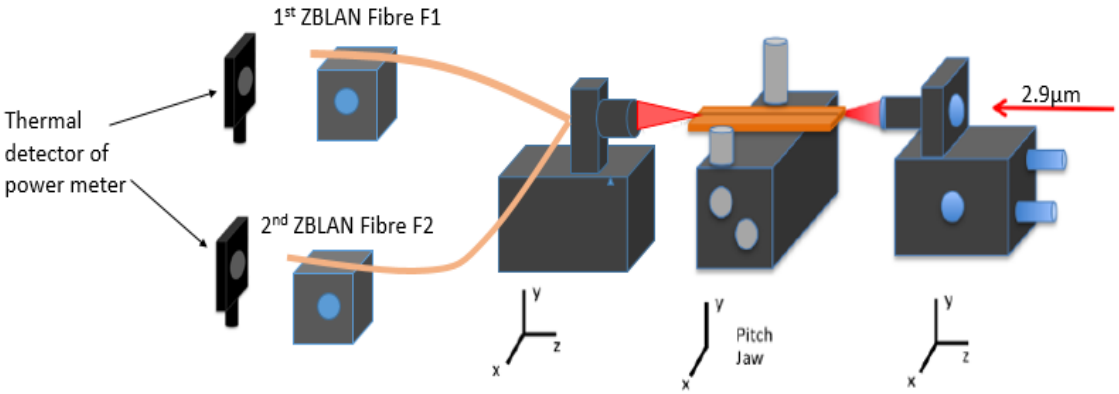

Figure 4.18 (a): A schematic setup used to test fibre coupled coupler

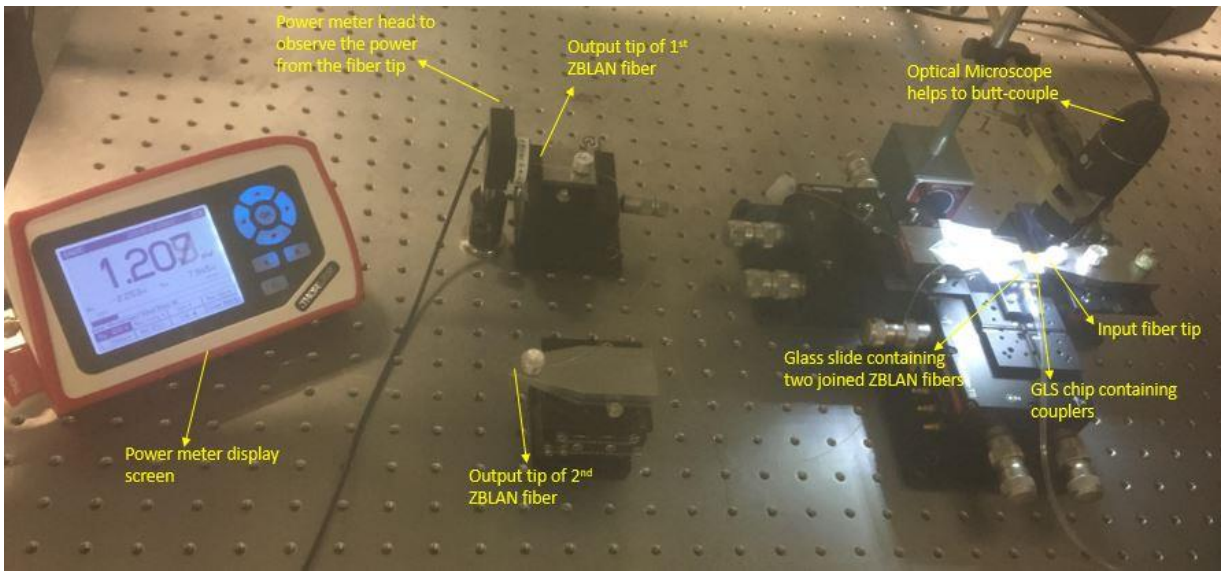

Figure 4.18(b): Actual lab setup used to test fibre-pigtailed coupler

There are two couplings that have to be considered at the same time.

- Coupling 1: From the input ZBLAN fibre to the coupler.
- Coupling 2: From the coupler to the output ZBLAN fibres.

The efficiency of Coupling 1 is not very high as the NA of the waveguides (0.090) in the couplers is lower than the NA of the input fibre (0.13). In contrast, Coupling 2 efficiency is high as now the NA of the waveguide is small but that of the collecting fibre is large so most of the light got coupled into the fibre from the coupler. This phenomenon is illustrated in Figure 4.19.

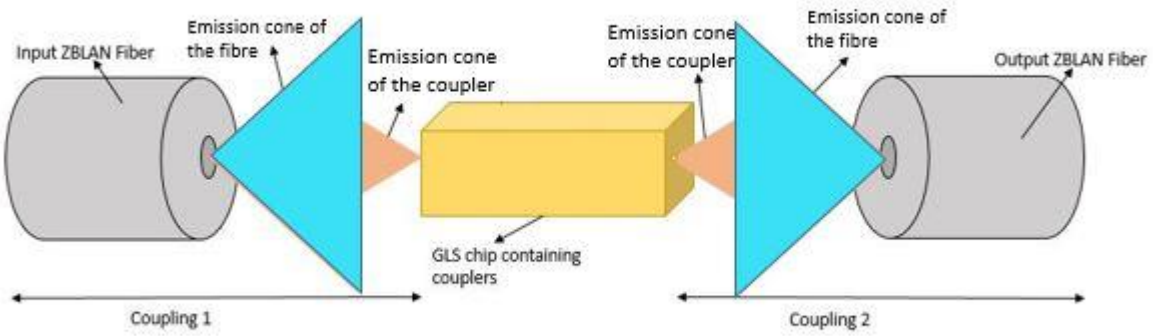

Figure 4.19: A Schematic diagram to illustrate the Coupling 1 and Coupling 2

The coupling efficiency of Coupling 2 is almost 70%. In the following table, the output ports of the coupler are named as Port P1 and Port P2 and the signal from these ports are coupled to the output

ZBLAN fibres joined together with glue. The output ends of these fibres where the power are measured is named 1st ZBLAN Fibre F1 and 2nd ZBLAN Fibre F2 as shown in figure 4.18 (a and b). In all the couplers, the same amount of coupling efficiency is observed. The values of two of the couplers are mentioned in Table 4.5(a & b).

(a)

Coupler outputs	Power (mW)	Output tips of ZBLAN Fibre	Power (mW)
Output Port P1	11	1st ZBLAN Fibre output F1	7.1
Output Port P2	1.2	2nd ZBLAN Fibre output F2	0.7

(b)

Coupler outputs	Power (mW)	Output tips of ZBLAN Fibre	Power (mW)
Output Port P1	5.01	1st ZBLAN Fibre F1	3.47
Output Port P2	5.61	2nd ZBLAN Fibre F2	3.81

Table 4.5(a and b): Power input and output values in coupling 2

The above table shows that when light is coupled into a single input port I_1 of the coupler, the signal at the output ports P1 and P2 is measured to be 11 mW and 1.2 mW respectively, see table 4.5(a). When these output signals are further coupled into the joined ZBLAN fibres, the signals at the output tips of the fibres are measured to be 7.1 mW and 0.7 mW. It can be seen that almost 70% of the signal light from the outputs of the coupler can be further coupled into a collecting ZBLAN fibre. Similar information is summarised in Table 4.5(b) for another coupler which has a more even distribution of power between the two ports.

4.6 Characterisation at the pump wavelength

The couplers were also tested for the pump wavelength (1.15 µm) of a $Ho^{3+:}$ Pr^{3+} co-doped ZBLAN Fibre. For this step, the laser output from a 1.15 µm diode was coupled into a silica fibre with 25 µm core diameter using the same setup mentioned earlier. The output light from the coupler was then

focused onto a silicon-based CCD camera (designed for 1.13 – 1.68 µm wavelength), instead of an IR camera as mentioned earlier for 2.9 µm, using a 20 mm focal length plano-convex lens. The coupler turned out to be multimode at the pump wavelength and the coupling ratio was found to be 100:0 at the pump wavelength that means no cross-coupling was observed at output port 2 compared to port 1. This means that the waveguide separation (24 µm and 26 µm) in the coupling region is not close enough for efficient evanescent wave coupling between the ports of the coupler at 1.15µm. As mentioned in Chapter 3 (Section3.6), Directional Couplers are wavelength dependent and, this has been confirmed here. For the signal wavelength (2.9 µm), the device is acting as a coupler whereas for the pump wavelength (1.15 µm) it is not. This is an advantageous for the use of these couplers as building blocks for a ring laser cavity as will be explained further in Chapter 5.

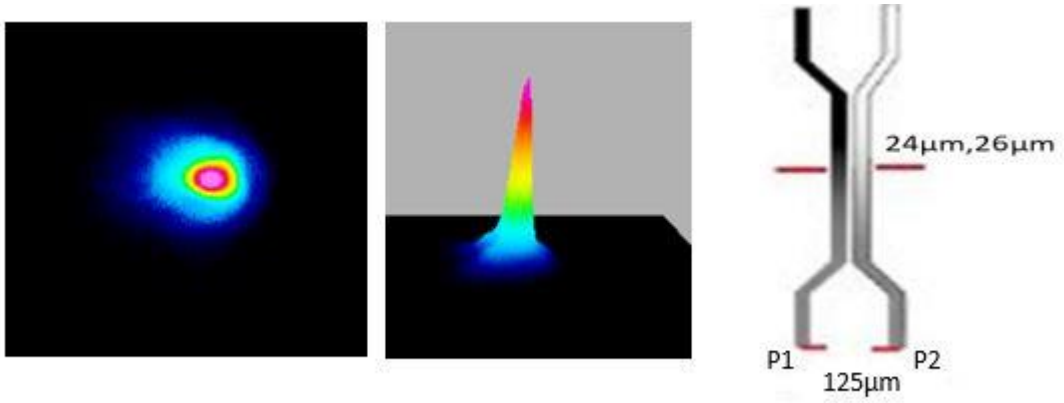

Figure 4.20: Image of the output facets of the GLS coupler at 1.15 µm, a schematic of a GLS coupler is shown in the right most picture.

The NA of the silica fibre used is 0.1 which is close enough to the NA of the waveguide (0.09) but the diameter of the core is 25µm which is larger than the width of the waveguide. It was thus expected to have smaller NA mismatch losses but higher MFD mismatch losses. Fresnel reflection on the chip interface can again be estimated as 1.80 dB using equation 4.1 where n_{GLS}= 2.38 at 1.15µm [54] and 2.29 at 2.9 µm respectively, n_{air}= 1. Various losses for the directional coupler at the pump wavelength 1.15 µm are shown in Table 4.6.

Various Losses	Loss in dB
NA mismatch Loss	0.91
MFD mismatch Loss	1.68
Fresnel Reflection Loss	1.8
Total Insertion loss	8.68
Propagation Loss/cm	4.3

Table 4.6: Measured and calculated losses of a coupler at pump 1.15 µm

It is evident from the results that the propagation loss is higher for the pump (1.15µm) than the signal (2.9 µm) wavelength. Again, careful evaluation is required to optimise the fabrication parameters to realise a low-loss waveguides coupler for the wavelengths 1.15µm and 2.9µm to demonstrate a fully integrated guided-wave ring laser cavity for the mid-IR.

4.7 Chapter Summary

In this chapter, the femtosecond laser inscription of waveguides into GLS glass has been detailed. Also, the fabrication of evanescent couplers and the characterisation of the waveguides and these couplers at 2.9 µm and 1.15 µm has been explained. Moreover, various losses have been calculated and presented in this chapter. It is evident from the results that in the testing chip the single track waveguides were single-moded at pulse energy 7 nJ to 12 nJ and multi-moded at 14nJ pulse energy. The double track waveguides having core to core separation 5.6 µm to 8.4 µm were reported to be single-moded whereas the one having 9.1 µm core to core separation was found to be at the edge of multimode. On the base of this data the new fabricated chip had triple tracks inscribed with laser pulse energies 10 nJ, 11 nJ, 12 nJ and 13 nJ and the triple tracks fabricated with the pulse energies 10 nJ and 11 nJ were reported to be single-mode only. In the initial chip, the NA mismatch loss was negligible (0.01 dB) and the MFD mismatch was a bit higher (0.14 dB) and the propagation loss/cm was reported up to 2.89 dB. In the new chip, the NA mismatch was found to be much higher (3.19dB) and the MFD mismatch (0.10dB) was reduced due to the fabrication of triple tracks and the propagation loss/cm was calculated up to 3.57 dB which was higher as compared to the value in the initial chip (2.89 dB). In conclusion, the MFD mismatch loss was decreased from 0.14 to 0.10 dB but the Numerical Aperture (NA) mismatch loss was increased from 0.01 to 3.19 dB. Numerical aperture of the fabricated waveguides is very crucial factor which cannot be neglected. Fabrication parameters need to be optimised to decrease the NA mismatch loss. In this project, the loss value for pump and signal both has not been decreased to a value where they can readily be used as a Wavelength Division Multiplexer (WDM) for a fully fibre integrated ring laser cavity, yet these calculations and results have provided guidelines for the future development of integrated mid-infrared components based on GLS glass.

5

Conclusion and Outlook

In conclusion, this project was an important step towards the development of a mid-IR-all-fibre laser system by fabricating an integrated optical component (directional coupler) in the mid-IR compatible glass GLS. The results are encouraging for the development of future all-fibre ring laser systems. Our results have shown that femtosecond laser inscribed GLS glass chips can be pig-tailed to mid-IR compatible fibres at the inputs and output ports of a directional coupler fibres if the losses at both input and output interfaces can be kept low. Our results at the output interface have shown 70% efficient coupling (from the GLS chip to the fibres) but at the input side coupling (fibre to the GLS chip) efficiency was limited by an NA mismatch. While these coupling losses are quite high at the moment, careful process optimisation will help to improve the efficiency. For example, an optimised composition of GLS could be used to increase the induced and thus the NA of the chip. In

addition, the actual fabrication parameters can be further optimised to achieve this goal. Eventually, these efforts will lead to the realisation of all-fibre ring laser cavities in the mid-IR region schematically shown in figure 5.1.

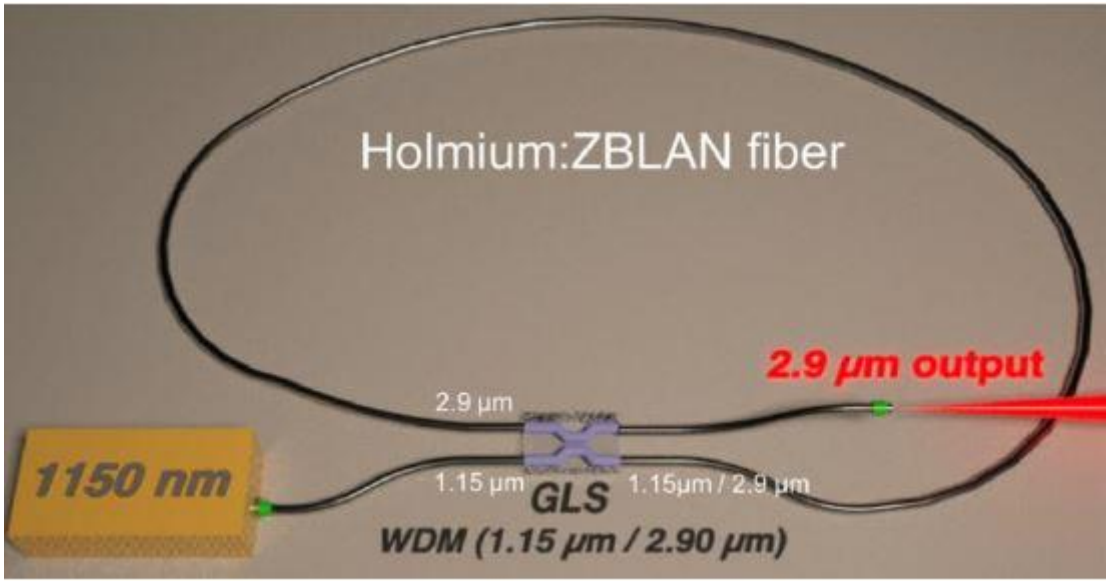

Figure 5.1: Schematic of a ring laser cavity

5.1 Future Works

The obvious first step for future work is to improve the design of GLS couplers to achieve a better coupling efficiency at 1150 nm and 2900 nm wavelengths and also use this coupler to build an efficient all-fibre mid-IR ring laser cavity. This, in turn, will establish a new platform technology for the creation of mid-infrared light sources that are fully integrated and thus field-deployable. As the mid-infrared part of the electromagnetic spectrum (2 – 20µm) holds the key to enable new solutions in spectroscopy, materials processing, chemical and bio-molecular sensing, security and industry [71], the development of real-world applications will be enabled by this research.

While fibre-based lasers have had an enormous impact in light-based technologies that are operating in the visible and near-infrared part of the electromagnetic spectrum, the development of mid-infrared fibre lasers for real-world applications is progressing at snail's pace due to the lack of integrated optical components in this crucially important spectral region as already mentioned in Section 1.1. Although GLS seems to be a suitable candidate for this task, in future, some new materials will also be explored.

A few research groups are already working on other different combination of glasses and are trying to find more and more reliable and efficient materials. For instance, a group recently presented BGG

(Barium Gallo Germanate) glass which upon femtosecond irradiation results in a positive refractive index change which makes it suitable for the fabrication of mid-IR photonic chips [62]. Also, although in ZBLAN glass there is always a negative index change observe it was recently found that when ZBLAN is modified by Hafnium (Hf), positive index change waveguides could be fabricated. This would be a breakthrough if directional couplers could be realized in ZBLAN, as an all ZBLAN glass laser cavity could be designed in this case [63].

Apart from representing an optimised pump/signal coupler, an evanescently-coupled 4-port device can also serve as a fundamental building block for an integrated nonlinear fibre loop mirror to generate ultra-short pulses out of a fibre laser oscillator [64].

References

[1] Schliesser A, Picqué N and Hänsch T W 2012 Mid-infrared frequency combs **6**

[2] Guastamacchia C 2009 Agnelli e lupi *Dent. Cadmos* **77** 5

[3] Bharathan G 2017 *Femtosecond Laser-Written Integrated Components for Future All-Fibre Mid-Infrared Laser Systems* (Macquarie University)

[4] Duling I N 1991 Subpicosecond all-fibre erbium laser *Electron. Lett.* **27** 544

[5] Anon Laser Fundamentals (2nd Edition) - Knovel

[6] Hu T 2009 *Ultrafast Mid-infrared Fibre Lasers* (University of Sydney)

[7] Snell J G, Citizen T, State T and Elderly T 2018 James G. Snell,

[8] Pourkazemi A and Mansourabadi M 2008 COMPARISON OF n fsm , n eff , AND THE SECOND AND THIRD ORDER DISPERSIONS OF PHOTONIC CRYSTAL FIBERS CALCULATED BY SCALAR EFFECTIVE INDEX METHOD AND EMPIRICAL RELATIONS METHODS *Prog. Electromagn. Res. M* **1** 197–206

[9] Hudson D D 2014 Invited paper: Short pulse generation in mid-IR fiber lasers *Opt. Fiber Technol.* **20** 631–41

[10] Jackson S D 2012 Towards high-power mid-infrared emission from a fibre laser *Nat. Photonics* **6** 423–31

[11] Bufetov I A and Dianov E M 2009 Bi-doped fiber lasers *Laser Phys. Lett.* **6** 487–504

[12] Snitzer E 1961 Optical Maser Action of Nd + 3 in a Barium Crown Glass *Phys. Rev. Lett.* **7** 444–6

[13] Philippe L, Doya V, Philippe R, Dominique P, Fabrice M and Olivier L 2003 Experimental study of pump power absorption along rare-earth-doped double clad optical fibres *Opt. Commun.* **218** 249–54

[14] Weber T, Liithy W, Weber H P, Neuman V, Berthou H and Kotrotsios G 1995 A longitudinal and side-pumped single transverse mode double-clad fiber laser with a special silicone coating *Opt. Commun.* **1** 5–99

[15] Koplow J P, Goldberg L and Kliner D A V 1998 Compact 1-W Yb-doped double-cladding fiber amplifier using V-groove side-pumping *IEEE Photonics Technol. Lett.* **10** 793–5

[16] Zenteno L 1993 High-power double-clad fiber lasers *J. Light. Technol.* **11** 1435–46

[17] Jeong Y, Sahu J K, Payne D N and Nilsson J 2004 Ytterbium-doped large-core fiber laser with 1.36 kW continuous-wave output power *Opt. Express* **12** 6088

[18] Allen R and Esterowitz L 1989 cw diode pumped 2.3 µm fiber laser *Cit. Appl. Phys. Lett* **55**

[19] Brierley M C and France P W 1988 Continuous wave lasing at 2.7 µm in an erbium-doped fluorozirconate fibrer *Electron. Lett.* **24** 935–7

[20] Henderson-sapir O, Munch J and Ottaway D J 2014 A Higher Power 3.5 µm Fibre Laser *Adv. Solid-State Lasers* 5–7

[21] Wetenkamp L 1990 Efficient CW operation of a 2.9 µm Ho3+-doped fluorozirconate fibre laser pumped at 640 nm *Electron. Lett.* **26** 883

[22] Carbonnier C, Tobben H and Unrau U B 1998 Room temperature CW fibre laser at 3.22 µm *Electron. Lett.* **34** 893–4

[23] Schneider J, Carbonnier C and B U 1997 Characterization of a Ho 3+ -doped uoride ber laser with a 3.9 µm emission wavelength *Appl. Opt.* **36** 8595–600

[24] Majewski M R and Jackson S D 2016 Highly efficient mid-infrared dysprosium fiber laser *Opt. Lett.* **41** 2173

[25] Antipov S, Hudson D D, Fuerbach A and Jackson S D 2016 High-power mid-infrared femtosecond fiber laser in the water vapor transmission window *Optica* **3** 1373

[26] Jackson S D 2004 Laser Operating At 2 . 86 Mm *Opt. Lett.* **29** 334–6
[27] Jackson S D 2009 High-power and highly efficient diode-cladding-pumped holmium-doped fluoride fiber laser operating at 294 µm *Opt. Lett.* **34** 2327
[28] Davis K M, Miura K, Sugimoto N and Hirao K 1996 Writing waveguides in glass with a femtosecond laser *Opt. Lett.* **21** 1729
[29] Cheng Y, Tsai H L, Sugioka K and Midorikawa K 2006 Fabrication of 3D microoptical lenses in photosensitive glass using femtosecond laser micromachining *Appl. Phys. A* **85** 11–4
[30] Bellouard Y, Said A, Dugan M and Bado P 2004 Fabrication of high-aspect ratio, micro-fluidic channels and tunnels using femtosecond laser pulses and chemical etching *Opt. Express* **12** 2120
[31] Bellouard Y, Said A A and Bado P 2005 Integrating optics and micro-mechanics in a single substrate: a step toward monolithic integration in fused silica *Opt. Express* **13** 6635
[32] Osellame R, Cerullo G and Ramponi R 2012 *Femtosecond Laser Micromachining: Photonic and Microfluidic Devices in Transparent Materials* vol 123
[33] Keldysh L V. 1965 Ionization in the Field of a Strong Electromagnetic Wave *J. Exp. Theor. Phys.* **20** 1307–14
[34] Zeng H 2015 *Ultrafast nonlinear optics* vol 3
[35] Gattass R R and Mazur E 2008 Femtosecond laser micromachining in transparent materials *Nat. Photonics* **2** 219–25
[36] Florea C and Winick K A 2003 Fabrication and characterization of photonic devices directly written in glass using femtosecond laser pulses *J. Light. Technol.* **21** 246–53
[37] Miura K, Qiu J, Inouye H, Mitsuyu T and Hirao K 1997 Photowritten optical waveguides in various glasses with ultrashort pulse laser *Appl. Phys. Lett.* **71** 3329–31
[38] Sudrie L, Franco M, Prade B and Mysyrowicz A 1999 Writing of permanent birefringent microlayers in bulk fused silica with femtosecond laser pulses *Opt. Commun.* **171** 279–84
[39] Sudrie L, Franco M, Prade B and Mysyrowicz A 2001 Study of damage in fused silica induced by ultra-short IR laser pulses *Opt. Commun.* **191** 333–9
[40] Glezer E N, Milosavljevic M, Huang L, Finlay R J, Her T-H, Callan J P and Mazur E 1996 Three-dimensional optical storage inside transparent materials *Opt. Lett.* **21** 2023
[41] Glezer E N and Mazur E 1997 Ultrafast-laser driven micro-explosions in transparent materials *Appl. Phys. Lett.* **71** 882–4
[42] Schaffer C B, Jamison A O and Mazur E 2004 Morphology of femtosecond laser-induced structural changes in bulk transparent materials *Appl. Phys. Lett.* **84** 1441–3
[43] Bricchi E, Klappauf B G and Kazansky P G 2004 Form birefringence and negative index change created by femtosecond direct writing in transparent materials *Opt. Lett.* **29** 119–21
[44] Shimotsuma Y, Kazansky P G, Qiu J and Hirao K 2003 Self-organized nanogratings in glass irradiated by ultrashort light pulses *Phys. Rev. Lett.* **91** 1–4
[45] Ams M and others 2009 Monolithic 100 mW Yb waveguide laser fabricated using the femtosecond-laser direct-write technique *Opt. Lett.* **34** 247–9
[46] Mauclair C, Mermillod-Blondin A, Huot N, Audouard E and Stoian R 2008 Ultrafast laser writing of homogeneous longitudinal waveguides in glasses using dynamic wavefront correction *Opt. Express* **16** 5481
[47] Gross S and Withford M J 2015 Ultrafast-laser-inscribed 3D integrated photonics: challenges and emerging applications *Nanophotonics* **4**
[48] Osellame R, Taccheo S, Marangoni M, Ramponi R, Laporta P, Polli D, De Silvestri S and Cerullo G 2003 Femtosecond writing of active optical waveguides with astigmatically shaped beams *J. Opt. Soc. Am. B* **20** 1559
[49] Schaffer C B, Brodeur A, García J F and Mazur E 2001 Micromachining bulk glass by use of femtosecond laser pulses with nanojoule energy *Opt. Lett.* **26** 93

[50] Chen W-J, Eaton S M, Zhang H and Herman P R 2008 Broadband directional couplers fabricated in bulk glass with high repetition rate femtosecond laser pulses *Opt. Express* **16** 11470
[51] Labadie L and Wallner O 2009 Mid-infrared guided optics: a perspective for astronomical instruments *Opt. Express* **17** 1947–62
[52] Paper C and Ambed B 2016 SCOPE OF CHALCOGENIDE GLASSES IN EMERGING SCIENCE & TECHNOLOGY [Review Article]
[53] Hewak D W, Brady D, Curry R J, Elliott G, Huang C C, Hughes M, Knight K, Mairaj A, Petrovich M N, Simpson R E and Sproat C 2010 Chalcogenide glasses for photonics device applications *Photonic Glas. Glas.* 29–102
[54] Advanced C and Partnership M 2015 GLS Infrared Transmitting Glass Datasheet **44** 0–1
[55] Requejo-Isidro J, Mairaj A K, Pruneri V, Hewak D W, Netti M C and Baumberg J J 2002 Self refractive non-linearities in chalcogenide based glasses *J. Non. Cryst. Solids* **317** 241–6
[56] Hughes M, Yang W and Hewak D 2007 Fabrication and characterization of femtosecond laser written waveguides in chalcogenide glass *Appl. Phys. Lett.* **90** 2005–8
[57] Streltsov A M and Borrelli N F 2001 Fabrication and analysis of a directional coupler written in glass by nanojoule femtosecond laser pulses *Opt. Lett.* **26** 42
[58] Gretzinger T, Gross S, Ams M, Arriola A and Withford M J 2015 Ultrafast laser inscription in chalcogenide glass: thermal versus athermal fabrication *Opt. Mater. Express* **5** 2862
[59] Gretzinger T, Gross S, Ams M, Arriola A and Withford M J 2016 Ultrafast laser waveguide inscription in Gallium Lanthanum Sulfide *Photonics Fiber Technol. 2016 (ACOFT, BGPP, NP)* AM4C.5
[60] Marcuse D 1976 Curvature loss formula for optical fibers *J. Opt. Soc. Am.* **66** 216
[61] Gross S, Lancaster D G, Ebendorff-Heidepriem H, Monro T M, Fuerbach A and Withford M J 2013 Femtosecond laser induced structural changes in fluorozirconate glass *Opt. Mater. Express* **3** 574
[62] Bérubé J-P, Le Camus A, Messaddeq S H, Petit Y, Messaddeq Y, Canioni L and Vallée R 2017 Femtosecond laser direct inscription of mid-IR transmitting waveguides in BGG glasses *Opt. Mater. Express* **7** 3124
[63] Heck M, Nolte S, Tünnermann A, Vallée R and Bernier M 2018 Femtosecond-written long-period gratings in fluoride fibers *Opt. Lett.* **43** 1994–7
[64] Doran N J and Wood D 1988 Nonlinear-optical loop mirror *Opt. Lett.* **13** 56
[65] https://www.thorlabs.com/tutorials.cfm?tabID=789B6970-20AC-47C3-81A9-838CD7594644
[66] https://www.photonics.com/a62269/Large-Mode- Area_Optical_Fibers_Maintain
[67] https://en.wikipedia.org/wiki/Double-clad_fiber
[68] K. Itoh, W. Watanabe, S. Nolte, and C. B. Schaffer, *MRS Bulletin*, 31, 620–625 (2006).
[69] https://www.mdpi.com/1424-8220/14/10/19402
[70] Loireau Lozac'h, A.M. ; Guittard, M. ; Flahaut, J.: Glasses formed by rare Earth Sulphides La_2S_3 with Gallium Sulphide Ga_2S_3. In: *Material Research Bulletin* 11 (1976), S. 1489-1496
[71] Nature Photonics Focus Issue: Mid-infrared Photonics, Nature Photonics, vol. 6, pp. 407-498 (2012)